Cover sheet

This is a preprint of a manuscript that is currently undergoing peer review. Subsequent versions of the manuscript may have different content. It has been written and published here to share experience and receive feedback. We invite you to contact us directly.

Kaihui Song (kaihuis@unc.edu)

Angel Hsu (angel.hsu@unc.edu)

Wei Peng (weipeng@princeton.edu)

Ying Yu (ying.yu@unc.edu)

Noah Kittner (kittner@email.unc.edu)

Projecting Future Heat Stress Disparities to 2100 in the Contiguous United States

Kaihui Song,[1]* Angel Hsu,[1] Wei Peng,[2,3] Ying Yu,[4] Noah Kittner[4,5]

[1] Data-Driven EnviroLab, School of Public Policy, University of North Carolina at Chapel Hill, Chapel Hill, NC 27599, USA.
[2] School of Public and International Affairs, Princeton University, Princeton, NJ 08540, USA.
[3] Andlinger Center For Energy and the Environment, Princeton University, Princeton, NJ 08540, USA.
[4] Department of Environmental Sciences and Engineering, Gillings School of Global Public Health, University of North Carolina at Chapel Hill, Chapel Hill, NC 27599, USA.
[5] Department of City and Regional Planning, University of North Carolina at Chapel Hill, Chapel Hill, NC 27599, USA.

* Kaihui Song (kaihuis@unc.edu)

Abstract

Global warming increases health risks from heat exposure. Historical evidence suggests disproportionate impacts of heat exposure in different regions across socioeconomic groups in the US. However, little is known about the scale of potential disparities and which populations stand to be most vulnerable under different future climate scenarios. Here, we assess county-level heat exposure, measured by Heat Index (HI) from now to 2100, in the contiguous US using an ensemble of Integrated Assessment Models results that present five future warming and socioeconomic development pathways. Our results reveal stark spatial and sociodemographic disparities in present and future heat stress, mainly for people of color and those aged 65 and older. The large proportion of high-risk populations residing in the Southern US makes this region particularly vulnerable to increases in HI, future climate warming will further enlarge disparities between presently-disadvantaged sociodemographic groups. Our findings underscore the need for considering sociodemographic factors when developing climate adaptation plans and prioritizing policy responses for vulnerable communities.

Introduction

Global warming has been shown to increase heat stress in human beings. Heatwaves, as an indicator of climate change impacts, have been increasing in frequency, duration, and intensity over the past five decades (*1*). Extreme temperatures pose profound threats to societies and human health (*2–6*). Increased temperatures, directly and indirectly, lead to a loss of agricultural productivity (*7*) and workplace efficiency (*8*, *9*), and increases in household energy consumption due to greater air conditioning demand (*10*). The recent decades have seen detrimental impacts on human health. An evident increase in mortality attributed to anthropogenic climate change, with approximately ~12,000 premature deaths occurring annually in the contiguous United States during the 2010s (*11*, *12*).

Historical evidence demonstrates that such heat-related impacts are unevenly distributed across regions and across different socioeconomic groups (*13*). Low-income, less educated neighborhoods within a US county are significantly hotter than the high-income and more

educated neighborhoods (*14*). Due to the Urban Heat Island (UHI) effect, cities are more exposed to excessive heat than rural areas. People of color and those living below poverty experience higher heat exposure and therefore more heat-related health risks than non-Hispanic White in wealthier areas throughout US cities (*15–18*). Significant racial urban heat disparities persist in 71% of US counties even when adjusting for income (*14*).

Earth System Models, relying on satellite observations, have been used to measure land surface temperature and associated frequency and intensity of heat waves with future climate change (*19*, *20*). What is unknown is the scale of potential impacts, which populations stand to be most vulnerable, and where disparities in heat exposure may be worsened, in these models. Existing studies exploring future heat exposure disparities mainly rely on downscaled higher spatial and temporal resolution-data to specific geographic or sociodemographic units in physical systems (*21–23*). For example, Dahl et al. (*21*) used downscaled climate models to project the frequency of population exposure to days exceeding National Weather Service-defined Heat Index risk thresholds, compared to a 1971-2000 baseline. Projected demographic and socioeconomic details, however, have yet to be considered in existing studies. Considering rapidly changing demographic and socioeconomic determinants, such as regional economic development and population migration, it is insufficient to assume a steady population composition to understand the disparity of impacts from excessive heat. Understanding who is affected by urban heating and what drives exposure disparities is therefore critical for crafting just and effective policy responses (*24*).

In this study, we aim to fill the existing research gap regarding the potential unequal impacts of future climate warming and heat stress on different demographic groups across the United States at the county level (n=3,108). We apply an integrated assessment modeling (IAM) framework to project future heat exposure and disparities based on varying sociodemographic factors across the contiguous US from 2020 to 2100. Utilizing the Coupled Model Intercomparison Project Phase 6 (CMIP 6), we project potential future temperature and relative humidity changes associated with various climate change pathways to identify locations in the US with rising heat stress by mid-century (2050) and by 2100. These data are then combined with five Shared Socioeconomic Pathways (SSPs) that provide different scenarios for future socioeconomic trends that allow us to project how future heat stress may disproportionately affect some populations over others, and what sociodemographic factors, such as race and ethnicity or age, contribute to future vulnerability to projected heat stress. We focus on the summer months (June, July, and August), since summer months on average are hotter than other periods throughout the year in North America and when populations may be at higher risk for heat-related health impacts. This framework allows us to understand where climate-induced heat stress is expected to affect populations, and which populations in which US counties may be most vulnerable to health impacts due to elevated heat exposure. Our results underscore the need for policymakers to pay attention to the vulnerabilities minority populations and older individuals will face under rising temperatures, as well as where these populations are distributed across the US.

Results

Heat projection in the contiguous US by 2100

Summer months (June, July and August) not only pose high heat-related health risks but also have higher increases in likelihood of heat disorders under high-emission climate scenarios (Table S4). For the entire contiguous US, we find projected Heat Index to be consistently

higher than anticipated increases in near-surface air temperature alone (Fig. 1A and 1B). The difference between near-surface air temperature and Heat Index is larger for higher-emission climate scenarios, such as SSP3-RCP7.0 and SSP5-RCP8.5 (Fig. 1C). When comparing projected median increases in Heat Index for summer months across counties under the SSP2-RCP4.5 scenario, which combines a "middle-of-the-road" socioeconomic pathway with moderate population growth and intermediate economic development, aligned with countries' current pledges (*25*), the Heat Index is projected to rise by 6.1°F (3.4°C) between 2020 and 2100. By 2100, under high-emission scenarios (SSP5-RCP8.5), the summer median increase in Heat Index may reach as high as 15.0°F (8.3 °C). These numbers are significantly higher than projected near-surface air temperature between 4.2 °F (2.3 °C) and 9.5 °F (5.3°C) for the same time period, mainly due to projected changes in relative humidity. The combined impact of near-surface air temperature and humidity results in a public health risk that potentially surpasses the risk posed by the projected increase in near-surface air temperature alone.

The per decade increases in near-surface air temperature and Heat Index show different spatial patterns (Fig. 1AB). Consistent with prior studies (*26*), higher latitudes experience a greater increase in near-surface air temperature; however, the increase in Heat Index is significantly higher in lower latitudes, especially in southeast coastal areas (Fig. 1D). Humidity levels play a critical role in heat perception in coastal areas, leading to an average increase of over 3°F at latitude 30°N under the SSP2-RCP4.5 scenario, with a difference exceeding 10°F compared to other latitudes. These findings suggest that individuals residing in the South may face not only heightened risks of heat exposure by 2100, indicated by high absolute values of Heat Index, but also the potential for a greater increase in Heat Index by 2050 and 2100.

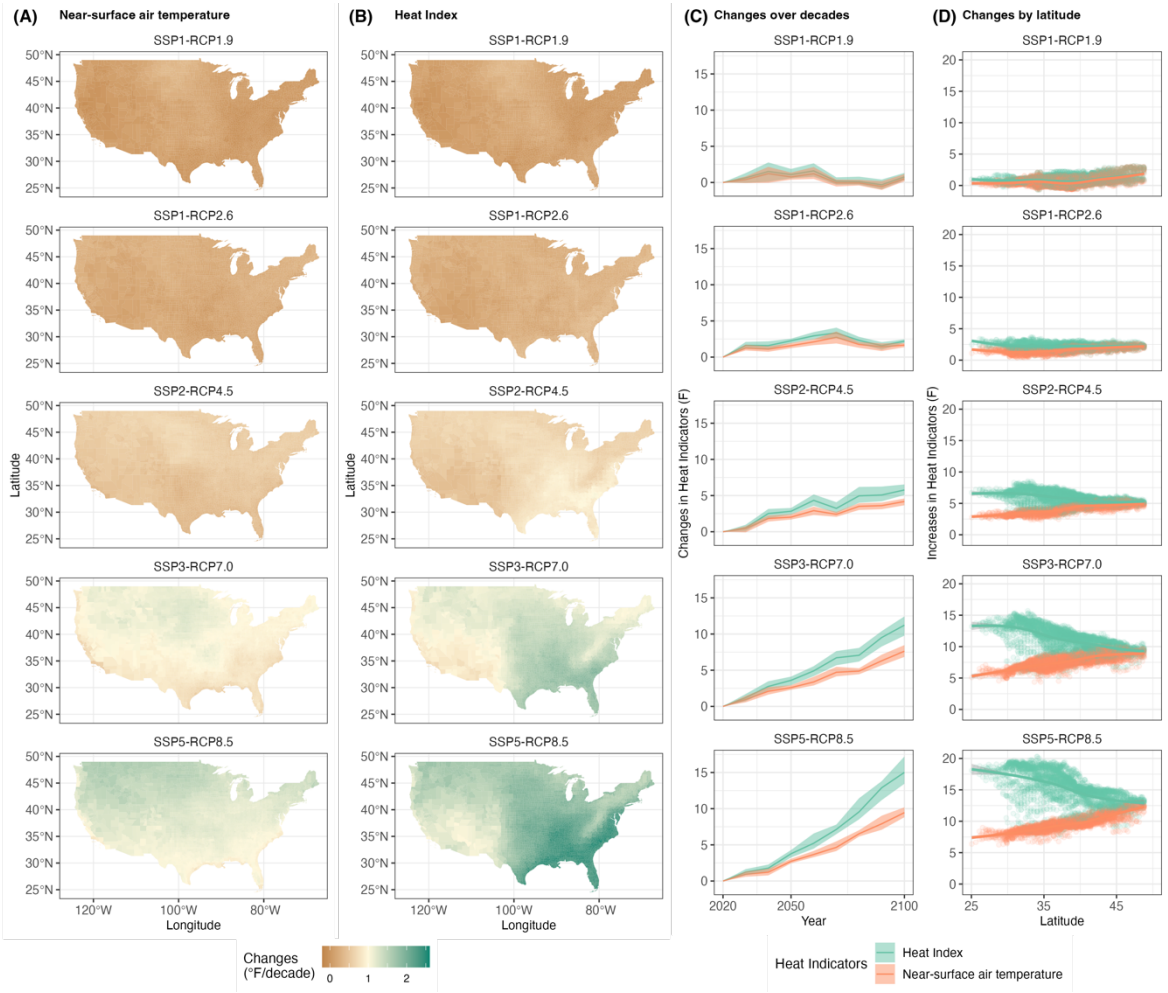

Fig. 1. Projected average heat index under five coupled SSP-RCP scenarios from 2020 to 2100. **(A)** per decade changes in near-surface air temperature at the county level; **(B)** per decade changes in Heat Index at county level; **(C)** median values of increases in heat indicators (near-surface air temperature vs. Heat Index); **(D)** changes in Heat Index by latitude.

Spatial heterogeneity of impacts

As shown in Fig. 2, the Heat Index data are categorized according to the social and health risks associated with "dangerous heat disorders with prolonged exposure and/or physical activity in the heat," as defined by the National Weather Service (NWS) (classification detail is presented in Table 1). Under higher-emission scenarios, a greater number of counties would fall into the at-risk categories (in *Caution*, *Extreme Caution* or *Danger* zones). In the low emissions scenario, following the sustainable development pathway (SSP1-RCP2.6), approximately half of the counties (50.6%) are projected to face risks by the mid-century (2045-2050). This percentage remains similar (51.1%) towards the end of the century (2095-2100) when compared to approximately 40% of counties at risk during the baseline period (2015-2020).

Under the middle of the road–intermediate GHG emissions scenario (SSP2-RCP4.5), the number of at-risk counties increases from ~40% to ~66% from the baseline period to the end of the century. By mid-century, this scenario will result in approximately 418 counties

(13.4% of total counties), home to an estimated population of around 43 million, to move from the *Safe to Caution* zone. An additional 355 counties (11.4% of total counties), where approximately 31 million people reside, will move from the *Caution* to *Extreme Caution* zone by the end of the century.

Under the high-emission scenario (SSP5-RCP8.5), only 8% of the counties will stay in the Safe zone by the 2100s, and one out of five counties will be in *Danger* zones. This scenario will pose risks to an additional 18 counties that will shift from the *Safe* to *Caution* zones by the middle of this century, and half of these counties (9 counties) will be placed in an *Extreme Caution* zone by the end of this century (detailed in Table S5). These counties are mainly located in Alabama, Colorado, Delaware, and Washington, DC. In addition, 161 counties, mainly located in Alabama, Arkansas, and Florida, where ~58 million people will reside by the end of this century, will face the risk of dangerous heat in the *Danger* zone. Notably, 85% of these counties were initially classified under the *Caution* zone during the baseline period.

The at-risk counties are primarily located in the Southern US, encompassing a total of 17 states stretching from Texas and Oklahoma in the west to Delaware in the east. The projected Heat Index under different climate scenarios indicates elevated HI levels across the Southern United States (see Table S7 for full US Census region definitions and Fig. S2 Fig. S3 for county details). By 2100, under the high-emission climate scenario (RCP8.5), the majority of people (97.8%) living in the Southern US will be classified as living in areas exposed to *Extreme Caution* and *Danger* zones. Even in the Northeast region, which includes 9 states and where future Heat Index is projected to be less severe than for lower latitudes due to lower relative humidity, 97.75% of the population living in this region in 2100 will experience Heat Index values consistent with the *Caution* and *Extreme Caution* ranges.

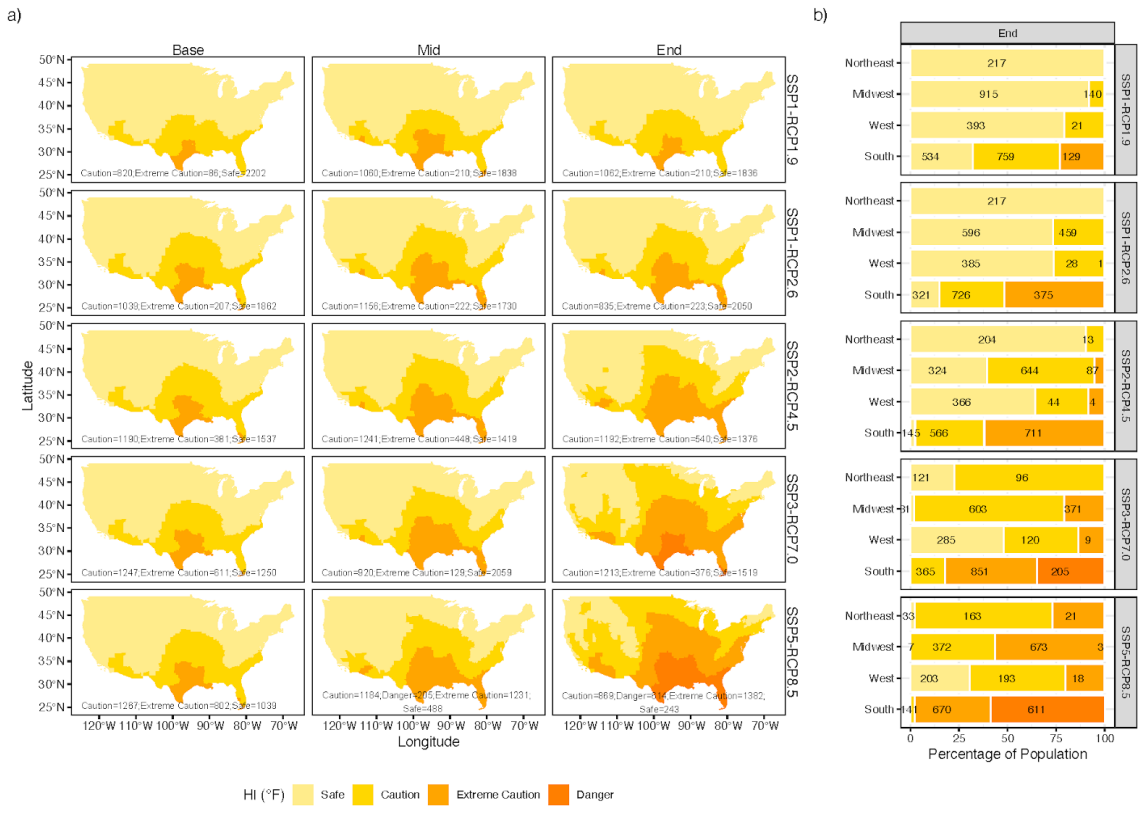

Fig. 2. Projected Heat Index, population and counties under five climate scenarios in the US. (A) Projected Heat Index under five climate scenarios in the US; **(B)** Percentage of population living in the four US regions by end of the century that will be located in Heat Index areas classified as *Safe*, *Caution*, *Extreme Caution*, and *Danger*, according to the National Weather Service (NWS) designations. Note: Base denotes the baseline years we used for comparison, average of 2015-2020; Mid means the middle of the century (average of 2045-2050), End means end of the century (average of 2095-2100); Labelled numbers on panels a and b refer to the number of counties in each NWS classification.

Sociodemographic disparities in heat exposure

Our research findings reveal a pronounced spatial heterogeneity in Heat Index across the contiguous United States, emphasizing the significant and escalating risks of heat exposure in the Southern region. In this section, we examine the population-weighted Heat Index by race, ethnicity, and age across various coupled SSP-RCP pathways. The results indicate that, currently, non-Hispanic Black populations experience an average temperature approximately ~3° F higher than non-Hispanic White populations (baseline period). The notable high absolute disparity between non-Hispanic Black and non-Hispanic White populations can be attributed, in part, to geographic location, as non-Hispanic Black populations predominantly reside in the South where the Heat Index remains high in all SSP-RCP scenarios and time periods considered. Presently (2015-2020), the majority (57.6%) of non-Hispanic Black populations reside in the South (historical data is mapped in Fig. 3A, future scenarios are shown in Fig. S6 and S7). This absolute disparity, determined by comparing HI values for non-Hispanic black populations and non-Hispanic white populations, exhibits an increasing trend by the 2100s under the high emission scenarios (SSP3-RCP7.0 and SSP5-RCP8.5) (Fig. 3B). The relative disparity, however, which indicates the rate of change in HI values, shows a slight decrease for the same time period (Fig. 3C). The reduced relative disparity is primarily attributed to the fact that Heat Index values increase ubiquitously across the contiguous US for all demographic groups.

Currently, non-White Hispanic populations experience the highest average Heat Index, however, both the absolute and relative disparity with non-Hispanic White populations are projected to decrease through 2100. Other races, mainly including Native Indian, Native Hawaiian and Asian populations, currently experience lower average Heat Index, mainly because Native Indian populations predominantly reside in the Midwest and Mountain regions of the US (e.g., Colorado, Utah, Montana, Nevada, Wyoming), where moderate increases in Heat Index are anticipated in the future (2050-2100). During the baseline periods (2015-2020), we observed a racial/ethnicity disparity in heat exposure across the US, where 63-65% of individuals in Safe zone were non-Hispanic White, whereas the percentage of the total population identified as White alone is less than 60%. In contrast, under the high-emission scenario (SSP5-RCP8.5) by the 2100s, approximately half (~48%) of the non-Hispanic White population is projected to remain in Safe Zones. This result stands in contrast to the fact that the non-Hispanic White individuals account for about 35% of the total population. The racial composition by Heat Index zone is shown in Fig. S4.

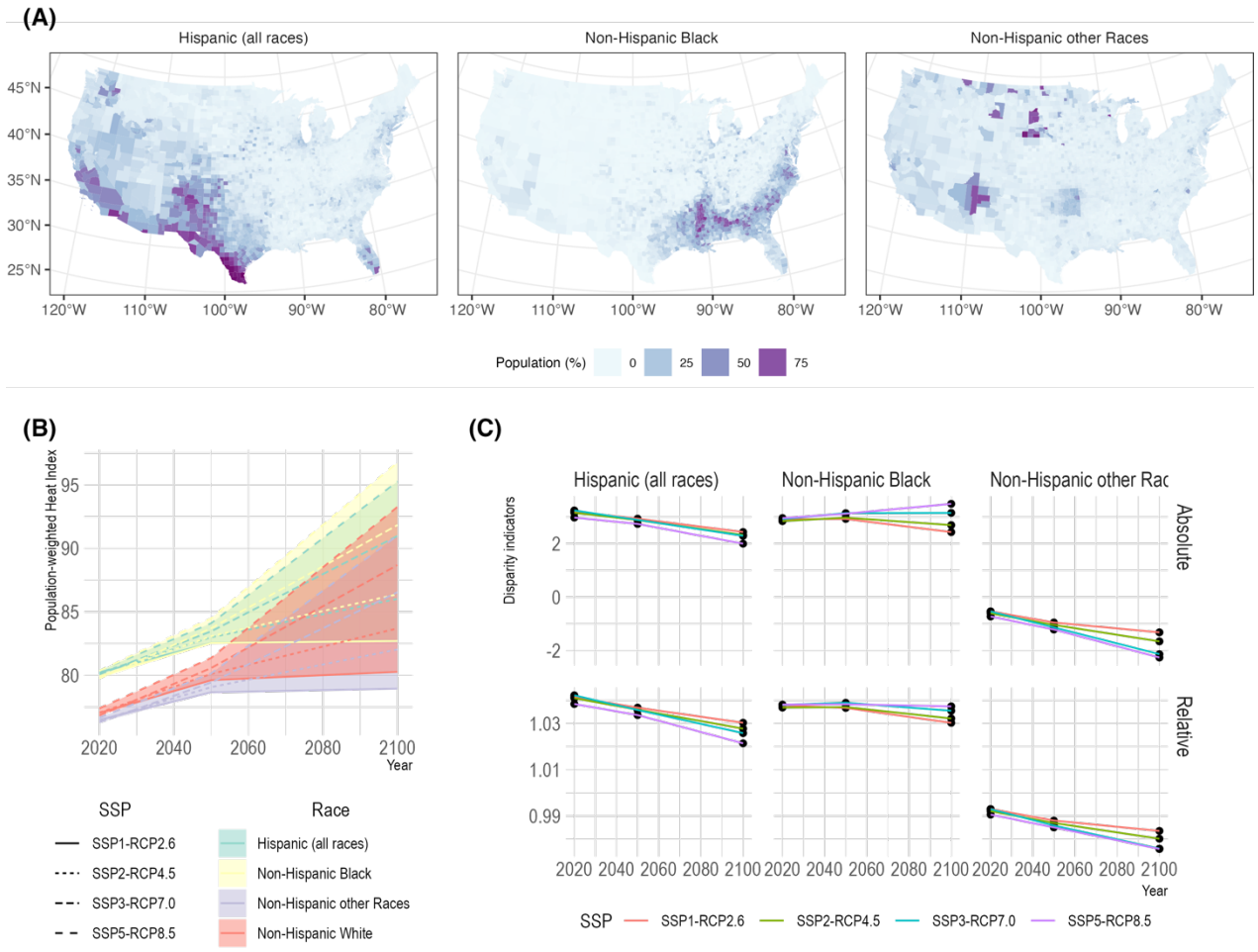

Fig. 3. Racial disparity of heat exposure under climate scenarios. **(A)** Racial composition from 2017-2021 5-year ACS data; **(B)** Population-weighted Heat Index by race/ethnicity; **(C)** Changes in racial disparity from heat exposure.

We further explored disparities across age groups under four coupled SSP-RCP scenarios and evaluated changes in absolute and relative disparities for the Adult populations (ages 20-65) over time (Fig. 4). Our results highlight that Elderly people (age 65+), on average, currently experience lower HI than the Adult population (Fig. 4B). However, in the future, there will be a disproportionate increase in HI for elderly populations aged 65 and above, with approximately 0.2 degree F higher HI compared to Adults. Since elderly populations are more affected by heat, a larger increase in Heat Index may pose higher health-related risks. This result is partially explained by aging populations located in the South, since we do not consider migration in the analysis (see Discussion).

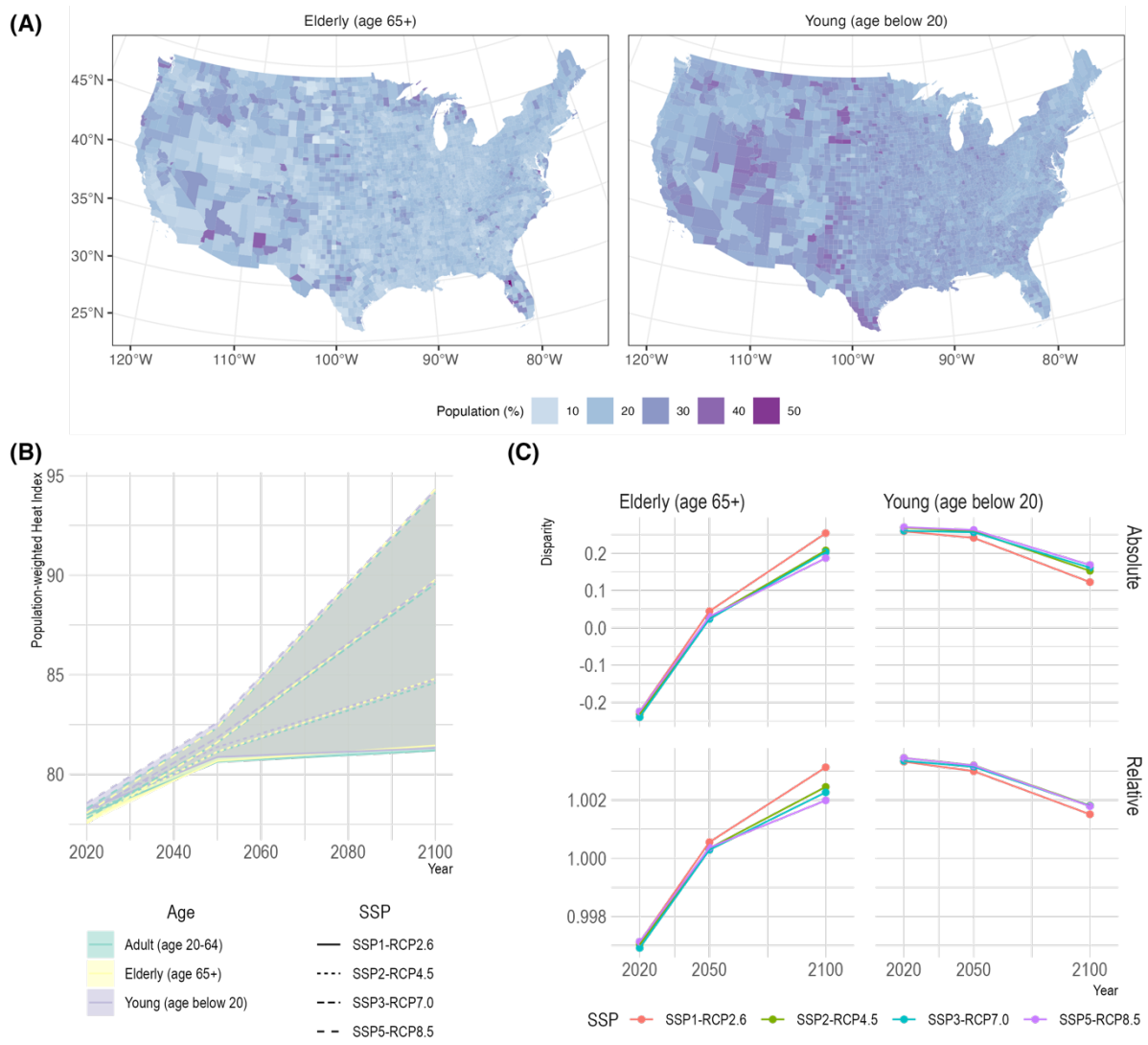

Fig. 4. Age disparity under four coupled SSP-RCP scenarios. **(A)** Age composition from 2017-2021 5-year ACS data; **(B)** Population-weighted Heat Index by age group under four coupled SSP-RCP scenarios. **(C)** Changes in absolute and relative disparity by age groups [Young (age <20), Adults (age 20-65), and Elderly (age 65+)] under four coupled SSP-RCP scenarios from 2020 to 2100.

Discussion

This paper has presented an analysis of future disparities in heat exposure for different sociodemographic groups from present-day to 2100 utilizing climate model scenarios that provide several possible trajectories of temperature rise, taking into consideration variations in population growth, economic development, and technological change that may impact greenhouse gas emissions and subsequent warming. To our knowledge, this study represents one of the first analyses that quantifies both the spatiotemporal and sociodemographic disparities in Heat Index, a combination of projected temperature and relative humidity, in US counties throughout the contiguous US. We find that counties in the South, where the highest proportion of people of color, namely non-Hispanic Black populations, experience the highest increases in HI over time as well as the greatest relative increases compared to other demographic groups, namely non-Hispanic White populations. In terms of age,

populations over the age of 65 will be disproportionately exposed to increased HI levels, compared to populations below the age of 65, in every scenario we examined.

These results underscore the need for understanding differences in underlying sociodemographic factors when evaluating future heat impacts and temperature changes due to climate change. We utilized state-of-the-art climate modeling and projection tools to evaluate future disparities in impacts, and below we discuss three considerations when applying these results for future studies or policy applications. First, our analysis stresses the importance of considering the spatial location of at-risk populations and their sociodemographics, which are co-located in the Southern US; second, we discuss the complexities of projecting Heat Index with Earth System models and limitations of our analysis; and third, we identify policy implications.

The Southern US stands to be most vulnerable to rising heat risks due to sociodemographic factors

Our findings consistently demonstrate that the Heat Index in the Southern US remains persistently high across different climate scenarios up until 2100. Although we did not take into account migration and the possibility that different racial, ethnic and age groups may substantially shift from present-day patterns, it is important to note that various SSP scenarios also do not make substantially distinct predictions regarding migration patterns or shifts in demographics (see Fig. S4). The counties with the highest HI increase are collocated with counties with higher percentages of non-Hispanic Black populations and people over the age of 65 across different SSP-RCP scenarios. However, it is important to note that our results still represent a conservative estimation since we use the monthly average Heat Index. Extreme heat days, which can exceed several standard deviations above the monthly average Heat Index, have the potential to pose even greater risks and disparities. Prior studies underscore that detrimental extreme heat events (e.g., heat waves) usually present extremely high temperatures over the course of a few days (*19*). Additionally, impacts of heat exposure are highly context-dependent, where local urban design (such as the shade of buildings or trees) plays a critical role in individuals' perception of heat stress (*20*).

Our estimation shows geographical overlaps between increases in Heat Index and demographics for both race and age, particularly in the Southern US, where the majority of the US non-Hispanic Black population and elderly are located. These demographic groups are documented to be more vulnerable to heat exposure (*27*, *28*). Through our disparity analysis, we have uncovered that non-Hispanic Black populations will experience more significant increases in Heat Index compared to other racial groups. Furthermore, in the worst-case climate warming scenarios, the gap between HI increases for non-Hispanic Black populations and non-Hispanic White populations widens over time. Other racial and ethnic groups do experience a smaller HI disparity gap compared to non-Hispanic white populations, and this gap narrows in the future in every scenario examined.

In terms of age, our study found the increasing gap in heat exposure between populations aged 65+ and those below underscores the need for greater attention to aging populations that will be at greater risk due to increasing HI. Existing studies have found that "people aged 65+ have been several times more likely to die from heat-related cardiovascular disease than the general population" (*29*). This finding underscores the critical need for prioritizing climate adaptation and mitigation strategies for elderly people, who stand to be at a greater risk of

heat-related health effects due to increased exposure to HI, compared to their younger, healthier counterparts (*6*, *30*).

Complexity of projecting Heat Index using Earth System models

Existing studies use different indicators to measure the impacts of increased temperature from climate change. The majority of the studies use remotely sensed land surface temperature (*14*, *15*, *31*) based on historical data or ESMs based on projected data (*26*, *32*), Heat Indices (*21*, *33*), and Wet Bulb Globe Temperature (WBGT). Our analyses reveal substantial disparities in both the magnitude of change and spatial patterns between near-surface air temperature and Heat Index, as used by National Weather Service. Our results confirm that global mean air temperature is nonlinearly related to heat stress, meaning that the same future warming experienced could trigger larger increases in societal and health impacts than documented using only surface temperature (*14*). Our results are also consistent with Chakraborty et al. (*34*), who found differences in the magnitude of disparities in heat exposure and stress when using different metrics, although consistent disparities were determined for populations of color and lower income. The selection of heat indicators should be guided by a study's specific objectives. When analyzing health impacts, the perception of heat, compared to land surface temperature, becomes a crucial indicator to consider. Additionally, it is worth considering whether the utilization of more comprehensive heat indicators can yield more robust and accurate projections results when estimating future outcomes.

When utilizing the model outputs of IAMs, it is important to consider various sources of uncertainty in the underlying model assumptions and their projected future scenarios. The Integrated Assessment Model Consortium (IAMC) plays a key role in standardizing inputs across various IAMs to enhance the comparability of model outputs. However, the difference in outputs is still influenced by parametric uncertainty, model structural uncertainty, and many uncertainties that cannot be fully captured (*35*). In our analyses, we employ an ensemble of model results to reduce uncertainty across models, although it does not completely eliminate overall uncertainty. In addition to IAMs' intrinsic uncertainty, there is also uncertainty in projecting population growth under different SSPs. These SSPs, widely used in scientific assessments like the IPCC Sixth Assessment Report, provide a framework for a set of five climate scenarios (detailed in Table S1). However, it is critical to acknowledge that the population projections within these scenarios introduce additional sources of uncertainty. To illustrate, we couple each climate scenario with a distinct Shared Socioeconomic Pathway (SSP) (Fig. 5), resulting in a range of population that will be impacted by the 2100s. Projections diverge sharply after 2050, partly due to the incorporation of alternative assumptions regarding key uncertain parameters, particularly at higher levels of population growth, productivity growth, and equilibrium climate sensitivity (*35*).

Precisely projecting heat-related impacts and inequality is even more challenging. Most Earth System Models and IAMs are developed at the global scale. National or state-level projections of HI are insufficient to analyze demographic disparities between different geographic populations. The migration of populations, which has not been factored into IAMs, represents one crucial factor. While scholars have developed methodologies and techniques to downscale the demographic composition to higher spatial resolutions, achieving precise results (such as census block level) is not guaranteed due to increased uncertainties associated with additional assumptions in the downscaling process. Analyzing demographic patterns at higher spatial resolutions, such as census tract or census block level, are impeded by data constraints.

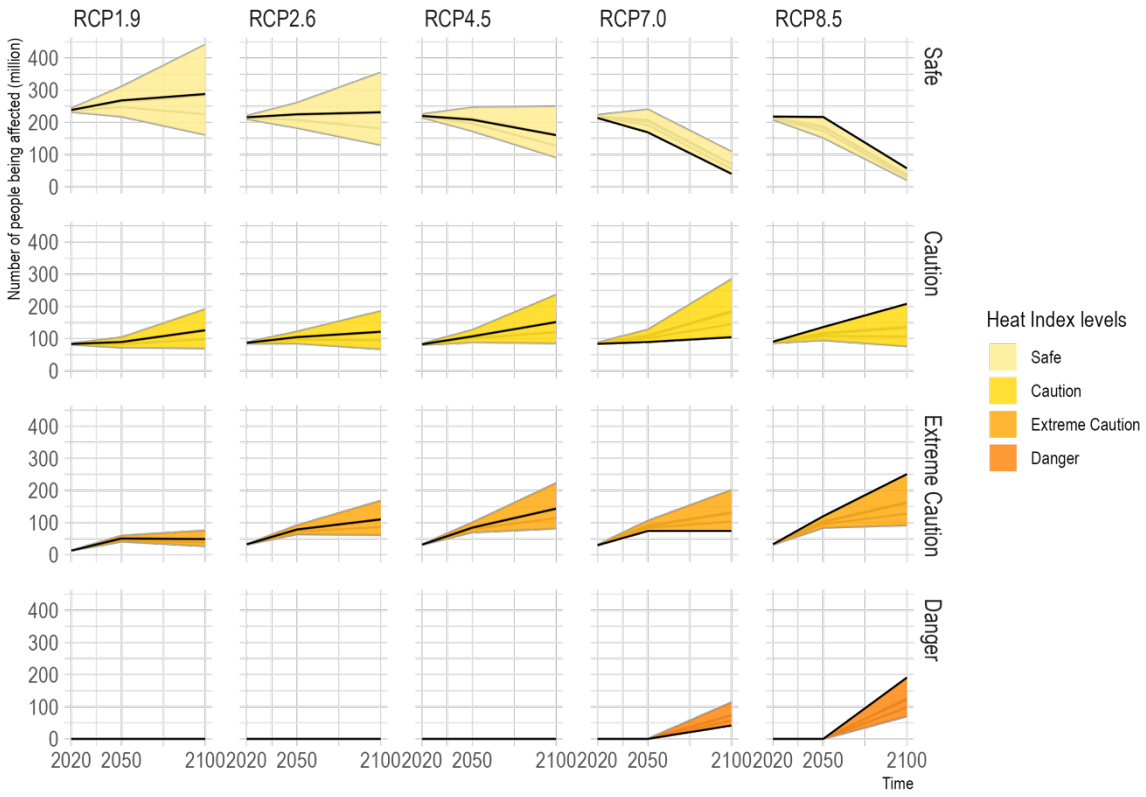

Fig. 5. Total number of people affected by heat stress from 2020 to 2100 [note: black line denotes the most likely coupled SSP-RCP scenarios (SSP1-RCP1.9, SSP1-RCP2.6, SSP2-RCP4.5, SSP3-RCP7.0, and SSP5-RCP8.5), while gray lines denote other coupled scenarios.

Designing just adaptation measures

The findings of our study highlight a consistent demographic disparity in future heat exposure, revealing greater and growing gaps in exposure for non-Hispanic Black populations and the Elderly, particularly in the Southern US, across all climate scenarios, even with a conservative estimation. Our analyses did not consider the adoption of additional adaptation measures, such as air conditioning, aggressive greening, and assumed no changes in vulnerability (e.g., other underlying health conditions that may become more chronic under climate change). Implementing preventive measures to address these disparities in heat exposure is critical to shaping the future climate policies to address what Frosch et al. refer to as the "climate gap," in which African American and Latino communities already face disproportionate health and economic consequences due to climate and environmental hazards (*36*). In addition, statistics also show that labor-intensive outdoor industries, such as manufacturing, are primarily located in the South (*37*, *38*), potentially posing higher health risks to labor forces and economic loss to society (*39*, *40*).

Analysis of mid and long-term impacts of climate-related heat exposure on different socioeconomic groups is crucial to develop adaptation plans at the local scale. According to (*41*), since just adaptation planning requires the inclusion of socially vulnerable populations, knowing where and whom these populations are is critical to engage them in processes that

ensure their involvement in planning decisions that ultimately affect them. With recent US federal policies like the Inflation Reduction Act earmarking specific funds to advance environmental and climate justice, cities and states have access to nearly $3 billion USD to "carry out environmental and climate justice activities to carry out environmental and climate justice activities to benefit underserved and overburdened communities" (*42*).

Materials and Methods

Data

Climate scenarios

Future climate projection data are obtained from the Scenario Model Intercomparison Project (ScenarioMIP) within the Coupled Model Intercomparison Project Phase 6 (CMIP6). By assembling 26 global climate and Earth system models (ESMs) in concentration-driven mode, which is indicated by RCPs, under five RCP scenarios, we obtained the median value of the Heat Index calculated by near-surface air temperature (*tas*) and relative humidity (*hurs*) under these climate scenarios at the standard 100km resolution. The multi-model ensemble reduces uncertainty associated with model choice. Table S1 describes four Tier 1 coupled SSP-RCP scenarios and an additional SSP1-RCP1.9 scenario (a scenario designed to limit global warming to 1.5 degree above 1850-1900) under the focus of this study. Models used to project Heat Index are listed in Table S2. In ScenarioMIP data, the projection under different climate scenarios is based on historical data from 1995 to 2014. We analyze the disparity of heat stress in baseline period (denoted as Base, using the mean of 2015-2020), middle of the century period (denoted as Mid, using the mean of 2045-2050) and end of the century period (denoted as End, using the mean of 2095-2100).

Socioeconomic data

To analyze the impacts of projected heat for different populations, we obtained socioeconomic data, including total population, gender, urbanization, race and age groups from multiple sources consistent with SSPs under RCP scenarios considered in this study at finer spatial resolution (detailed in Table S3). We then aggregated the downscaled socioeconomic data into the county level to analyze the impacts of future heat stress on different socioeconomic groups. Given the lack of credibility in income projection data, we did not examine future disparities between different income groups.

Heat index

Heat metrics, which typically combine several indicators of heat stress including air temperature and humidity, can inform measures that need to be taken to avoid health risks. We employ Heat Index (HI) because of its relevance to increasing morbidity and mortality risk as a consequence of global warming. Additionally, the availability of newly acquired data enables us to provide fine-scale estimates spanning until the end of this century. Among the wide array of over 20 different heat indices in the literature, we chose to use the US National Weather Service (NWS) Heat Index). This particular HI has demonstrated superior performance when compared to algorithms approximating Steadman's original apparent temperature values (*43*). Based on Steadman's theory, Lans P. Rothfusz performed multiple regression analyses, described in a 1990 NWS Technical Attachment (SR 90-23). This HI is widely used in heat warning systems and environmental health research and the relevant health risk is shown in Table 1.

Table 1 Heat index and its relevance to public health risks

Classification	Heat Index	Effect on the human body
Caution	80°F - 90°F	Fatigue possible with prolonged exposure and/or physical activity
Extreme Caution	90°F - 103°F	Heat stroke, heat cramps, or heat exhaustion possible with prolonged exposure and/or physical activity
Danger	103°F - 124°F	Heat cramps or heat exhaustion likely, and heat stroke possible with prolonged exposure and/or physical activity
Extreme Danger	125°F or higher	Heat stroke highly likely

(Source: National Weather Services)

This HI is based on air temperature and air moisture. In our study, we use the projected near-surface temperature (*tas*) and projected surface relative humidity (*hurs*) derived from multiple models from CMIP6 database to calculate heat index under different climate change scenarios. The calculation of HI is performed using R package *weathermetrics* developed by Anderson et al. (*44*).

Disparity indicators

We calculated population-weighted HI in summer months (average HI for June, July, August for the median value of the output from various ESMs) in the contiguous US by each socio-demographic group i for a given year, as follows:

$$h_i = \frac{\sum_{j=1}^{n} c_j p_{ij}}{\sum_{j=1}^{n} p_{ij}}$$

where, c_j is the projected average Heat Index for county j, p_{ij} is the projected population of demographic group i in county j.

Based on the population-weighted HI, we provide a measure of overall racial/ethnicity disparities considering all counties at the national level. The absolute disparity is calculated as the HI difference between demographic groups and, similarly, the relative disparity is calculated using the ratio between demographic groups. Specifically, the racial disparity measures the disparity of non-Hispanic Black, Hispanic (all races), and non-Hispanic Other Races against non-Hispanic White population, while the age disparity measures the disparity of Elderly population (age 65+) and Young population (age<20) against the Adult group (age 20-65). The absolute and relative disparities have been used in many studies (*45–47*) to measure sociodemographic differences.

The absolute disparity and relative disparity for a given year are calculated as:

Absolute disparity = $h_{i,i\neq c} - h_c$

Relative disparity = $\frac{h_{i,i\neq c}}{h_c}$

where c denotes the compared demographic groups, i.e. non-Hispanic White and Adults (age 20-65).

References

1. EPA, Climate Change Indicators: Heat Waves (2022), (available at https://www.epa.gov/climate-indicators/climate-change-indicators-heat-waves).
2. S. M. Hsiang, M. Burke, E. Miguel, Quantifying the Influence of Climate on Human Conflict. *Science (1979)*. **341** (2013), doi:10.1126/science.1235367.
3. M. Burke, S. M. Hsiang, E. Miguel, Global non-linear effect of temperature on economic production. *Nature*. **527**, 235–239 (2015).
4. J. Yang, M. Zhou, Z. Ren, M. Li, B. Wang, D. L. Liu, C.-Q. Ou, P. Yin, J. Sun, S. Tong, H. Wang, C. Zhang, J. Wang, Y. Guo, Q. Liu, Projecting heat-related excess mortality under climate change scenarios in China. *Nat Commun*. **12**, 1039 (2021).
5. Y. Fan, L. Pei-Syuan, E.-S. Im, M.-H. Lo, Regional disparities in the exposure to heat-related mortality risk under 1.5 °C and 2 °C global warming. *Environmental Research Letters*. **17**, 054009 (2022).
6. K. L. Ebi, A. Capon, P. Berry, C. Broderick, R. de Dear, G. Havenith, Y. Honda, R. S. Kovats, W. Ma, A. Malik, N. B. Morris, L. Nybo, S. I. Seneviratne, J. Vanos, O. Jay, Hot weather and heat extremes: health risks. *The Lancet*. **398**, 698–708 (2021).
7. C. Lesk, W. Anderson, A. Rigden, O. Coast, J. Jägermeyr, S. McDermid, K. F. Davis, M. Konar, Compound heat and moisture extreme impacts on global crop yields under climate change. *Nat Rev Earth Environ*. **3**, 872–889 (2022).
8. C. He, Y. Zhang, A. Schneider, R. Chen, Y. Zhang, W. Ma, P. L. Kinney, H. Kan, The inequality labor loss risk from future urban warming and adaptation strategies. *Nat Commun*. **13**, 3847 (2022).
9. D. García-León, A. Casanueva, G. Standardi, A. Burgstall, A. D. Flouris, L. Nybo, Current and projected regional economic impacts of heatwaves in Europe. *Nat Commun*. **12**, 5807 (2021).
10. B. J. van Ruijven, E. De Cian, I. Sue Wing, Amplification of future energy demand growth due to climate change. *Nat Commun*. **10**, 2762 (2019).
11. A. M. Vicedo-Cabrera, N. Scovronick, F. Sera, D. Royé, R. Schneider, A. Tobias, C. Astrom, Y. Guo, Y. Honda, D. M. Hondula, R. Abrutzky, S. Tong, M. de S. Z. S. Coelho, P. H. N. Saldiva, E. Lavigne, P. M. Correa, N. V. Ortega, H. Kan, S. Osorio, J. Kyselý, A. Urban, H. Orru, E. Indermitte, J. J. K. Jaakkola, N. Ryti, M. Pascal, A. Schneider, K. Katsouyanni, E. Samoli, F. Mayvaneh, A. Entezari, P. Goodman, A. Zeka, P. Michelozzi, F. de'Donato, M. Hashizume, B. Alahmad, M. H. Diaz, C. D. L. C. Valencia, A. Overcenco, D. Houthuijs, C. Ameling, S. Rao, F. Di Ruscio, G. Carrasco-Escobar, X. Seposo, S. Silva, J. Madureira, I. H. Holobaca, S. Fratianni, F. Acquaotta, H. Kim, W. Lee, C. Iniguez, B. Forsberg, M. S. Ragettli, Y. L. L. Guo, B. Y. Chen, S. Li, B. Armstrong, A. Aleman, A. Zanobetti, J. Schwartz, T. N. Dang, D. V. Dung, N. Gillett, A. Haines, M. Mengel, V. Huber, A. Gasparrini, The burden of heat-related mortality attributable to recent human-induced climate change. *Nat Clim Chang*. **11**, 492–500 (2021).
12. D. Shindell, Y. Zhang, M. Scott, M. Ru, K. Stark, K. L. Ebi, The Effects of Heat Exposure on Human Mortality Throughout the United States. *Geohealth*. **4** (2020), doi:10.1029/2019GH000234.
13. N. S. Diffenbaugh, M. Burke, Global warming has increased global economic inequality. *Proceedings of the National Academy of Sciences*. **116**, 9808–9813 (2019).
14. S. A. Benz, J. A. Burney, Widespread Race and Class Disparities in Surface Urban Heat Extremes Across the United States. *Earths Future*. **9** (2021), doi:10.1029/2021EF002016.
15. A. Hsu, G. Sheriff, T. Chakraborty, D. Manya, Disproportionate exposure to urban heat island intensity across major US cities. *Nat Commun*. **12**, 2721 (2021).
16. T. Chakraborty, A. Hsu, D. Manya, G. Sheriff, Disproportionately higher exposure to urban heat in lower-income neighborhoods: a multi-city perspective. *Environmental Research Letters*. **14**, 105003 (2019).
17. T. Chakraborty, A. Hsu, D. Manya, G. Sheriff, A spatially explicit surface urban heat island database for the United States: Characterization, uncertainties, and possible applications. *ISPRS Journal of Photogrammetry and Remote Sensing*. **168**, 74–88 (2020).

18. J. S. Hoffman, V. Shandas, N. Pendleton, The Effects of Historical Housing Policies on Resident Exposure to Intra-Urban Heat: A Study of 108 US Urban Areas. *Climate*. **8**, 12 (2020).
19. T. L. Frölicher, C. Laufkötter, Emerging risks from marine heat waves. *Nat Commun*. **9**, 650 (2018).
20. Z. Zheng, L. Zhao, K. W. Oleson, Large model structural uncertainty in global projections of urban heat waves. *Nat Commun*. **12**, 3736 (2021).
21. K. Dahl, R. Licker, J. T. Abatzoglou, J. Declet-Barreto, Increased frequency of and population exposure to extreme heat index days in the United States during the 21st century. *Environ Res Commun*. **1**, 075002 (2019).
22. Y. Chen, X. Qin, The Impact of Extreme Temperature Shocks on the Health Status of the Elderly in China. *Int J Environ Res Public Health*. **19**, 15729 (2022).
23. Y. T. E. Lo, D. M. Mitchell, A. Gasparrini, A. M. Vicedo-Cabrera, K. L. Ebi, P. C. Frumhoff, R. J. Millar, W. Roberts, F. Sera, S. Sparrow, P. Uhe, G. Williams, Increasing mitigation ambition to meet the Paris Agreement's temperature goal avoids substantial heat-related mortality in U.S. cities. *Sci Adv*. **5** (2019), doi:10.1126/sciadv.aau4373.
24. F.-A. Hoover, S. Meerow, Z. J. Grabowski, T. McPhearson, Environmental justice implications of siting criteria in urban green infrastructure planning. *Journal of Environmental Policy & Planning*. **23**, 665–682 (2021).
25. D. P. van Vuuren, T. R. Carter, Climate and socio-economic scenarios for climate change research and assessment: reconciling the new with the old. *Clim Change*. **122**, 415–429 (2014).
26. R. S. Vose, D. R. Easterling, K. E. Kunkel, A. N. LeGrande, M. F. Wehner, "Ch. 6: Temperature Changes in the United States. Climate Science Special Report: Fourth National Climate Assessment, Volume I" (Washington, DC, 2017), , doi:10.7930/J0N29V45.
27. J. Wang, Y. Chen, W. Liao, G. He, S. F. B. Tett, Z. Yan, P. Zhai, J. Feng, W. Ma, C. Huang, Y. Hu, Anthropogenic emissions and urbanization increase risk of compound hot extremes in cities. *Nat Clim Chang*. **11**, 1084–1089 (2021).
28. J. Hess, Heat and health inequity: acting on determinants of health to promote heat justice. *Nat Rev Nephrol*. **19**, 143–144 (2023).
29. EPA, Climate change indicators heat-related deaths (2021), (available at https://www.epa.gov/climate-indicators/climate-change-indicators-heat-related-deaths).
30. G. P. Kenny, J. Yardley, C. Brown, R. J. Sigal, O. Jay, Heat stress in older individuals and patients with common chronic diseases. *Can Med Assoc J*. **182**, 1053–1060 (2010).
31. C. Wobus, C. Zarakas, P. Malek, B. Sanderson, A. Crimmins, M. Kolian, M. Sarofim, C. P. Weaver, Reframing Future Risks of Extreme Heat in the United States. *Earths Future*. **6**, 1323–1335 (2018).
32. J. Ban, K. Lu, Q. Wang, T. Li, Climate change will amplify the inequitable exposure to compound heatwave and ozone pollution. *One Earth*. **5**, 677–686 (2022).
33. First Street Foundation, "The 6th National Risk Assessment: Hazardous Heat" (2022).
34. T. Chakraborty, A. J. Newman, Y. Qian, A. Hsu, G. Sheriff, Residential segregation and outdoor urban moist heat stress disparities in the United States. *One Earth*. **6**, 738–750 (2023).
35. K. Gillingham, W. Nordhaus, D. Anthoff, G. Blanford, V. Bosetti, P. Christensen, H. McJeon, J. Reilly, Modeling Uncertainty in Integrated Assessment of Climate Change: A Multimodel Comparison. *J Assoc Environ Resour Econ*. **5**, 791–826 (2018).
36. R. Morello-Frosch, O. K. Obasogie, The Climate Gap and the Color Line — Racial Health Inequities and Climate Change. *New England Journal of Medicine*. **388**, 943–949 (2023).
37. The Conference Board, Rates of remote work widely across US States (2021), (available at https://www.conference-board.org/topics/natural-disasters-pandemics/remote-work-us).
38. BLS, ccupational Employment and Wage Statistics (2023).
39. L. A. Parsons, D. Shindell, M. Tigchelaar, Y. Zhang, J. T. Spector, Increased labor losses and decreased adaptation potential in a warmer world. *Nat Commun*. **12**, 7286 (2021).
40. K. K. Zander, W. J. W. Botzen, E. Oppermann, T. Kjellstrom, S. T. Garnett, Heat stress causes substantial labour productivity loss in Australia. *Nat Clim Chang*. **5**, 647–651 (2015).
41. J. T. Malloy, C. M. Ashcraft, A framework for implementing socially just climate adaptation. *Clim Change*. **160**, 1–14 (2020).

42. EPA, Inflation Reduction Act Environmental and Climate Justice Program (2023).
43. R. G. Steadman, A Universal Scale of Apparent Temperature. *Journal of Climate and Applied Meteorology*. **23**, 1674–1687 (1984).
44. G. B. Anderson, M. L. Bell, R. D. Peng, Methods to Calculate the Heat Index as an Exposure Metric in Environmental Health Research. *Environ Health Perspect*. **121**, 1111–1119 (2013).
45. J. Liu, L. P. Clark, M. J. Bechle, A. Hajat, S.-Y. Kim, A. L. Robinson, L. Sheppard, A. A. Szpiro, J. D. Marshall, Disparities in Air Pollution Exposure in the United States by Race/Ethnicity and Income, 1990–2010. *Environ Health Perspect*. **129** (2021), doi:10.1289/EHP8584.
46. S. Harper, E. Ruder, H. Roman, A. Geggel, O. Nweke, D. Payne-Sturges, J. Levy, Using Inequality Measures to Incorporate Environmental Justice into Regulatory Analyses. *Int J Environ Res Public Health*. **10**, 4039–4059 (2013).
47. A. Jbaily, X. Zhou, J. Liu, T.-H. Lee, L. Kamareddine, S. Verguet, F. Dominici, Air pollution exposure disparities across US population and income groups. *Nature*. **601**, 228–233 (2022).
48. C. Tebaldi, K. Debeire, V. Eyring, E. Fischer, J. Fyfe, P. Friedlingstein, R. Knutti, J. Lowe, B. O'Neill, B. Sanderson, D. van Vuuren, K. Riahi, M. Meinshausen, Z. Nicholls, K. B. Tokarska, G. Hurtt, E. Kriegler, J.-F. Lamarque, G. Meehl, R. Moss, S. E. Bauer, O. Boucher, V. Brovkin, Y.-H. Byun, M. Dix, S. Gualdi, H. Guo, J. G. John, S. Kharin, Y. Kim, T. Koshiro, L. Ma, D. Olivié, S. Panickal, F. Qiao, X. Rong, N. Rosenbloom, M. Schupfner, R. Séférian, A. Sellar, T. Semmler, X. Shi, Z. Song, C. Steger, R. Stouffer, N. Swart, K. Tachiiri, Q. Tang, H. Tatebe, A. Voldoire, E. Volodin, K. Wyser, X. Xin, S. Yang, Y. Yu, T. Ziehn, Climate model projections from the Scenario Model Intercomparison Project (ScenarioMIP) of CMIP6. Earth System Dynamics. 12, 253–293 (2021).
49. B. C. O'Neill, C. Tebaldi, D. P. van Vuuren, V. Eyring, P. Friedlingstein, G. Hurtt, R. Knutti, E. Kriegler, J.-F. Lamarque, J. Lowe, G. A. Meehl, R. Moss, K. Riahi, B. M. Sanderson, The Scenario Model Intercomparison Project (ScenarioMIP) for CMIP6. Geosci Model Dev. 9, 3461–3482 (2016).
50. J. Gao, M. Pesaresi, Downscaling SSP-consistent global spatial urban land projections from 1/8-degree to 1-km resolution 2000–2100. Sci Data. 8, 281 (2021).
51. M. E. Hauer, Population projections for U.S. counties by age, sex, and race controlled to shared socioeconomic pathway. Sci Data. 6, 190005 (2019).
52. D. Murakami, T. Yoshida, Y. Yamagata, Gridded GDP Projections Compatible With the Five SSPs (Shared Socioeconomic Pathways). Front Built Environ. 7 (2021), doi:10.3389/fbuil.2021.760306.

Supplementary Materials for

Projecting Future Heat Stress Disparities to 2100 in the Contiguous United States

Kaihui Song,[1]* Angel Hsu,[1] Wei Peng,[2,3] Ying Yu,[4] Noah Kittner[4,5]

[1] Data-Driven EnviroLab, School of Public Policy, University of North Carolina at Chapel Hill, Chapel Hill, NC 27599, USA.
[2] School of Public and International Affairs, Princeton University, Princeton, NJ 08540, USA.
[3] Andlinger Center for Energy and the Environment, Princeton University, Princeton, NJ 08540, USA.
[4] Department of Environmental Sciences and Engineering, Gillings School of Global Public Health, University of North Carolina at Chapel Hill, Chapel Hill, NC 27599, USA.
[5] Department of City and Regional Planning, University of North Carolina at Chapel Hill, Chapel Hill, NC 27599, USA.

*Corresponding author: Kaihui Song (email: kaihuis@unc.edu)

Supplementary data description

1 CMIP6 models

CMIP6 (Coupled Model Intercomparison Project 6): We obtain near-surface air temperature (2m above the ground) (*tas*) and corresponding relative humidity (*hurs*) from ScenarioMIP in CMIP6. This database provides a range of outcomes based on concentration-driven simulations from participating global coupled Earth System Models (*1*). ScenarioMIP specifically provides multi-model climate projections based on different scenarios with future emissions and land use changes produced with Integrated Assessment Models, using 1995-2014 as historical baseline for simulations (*2*). Figure S1 illustrated the coupled SSP-RCP simulations in CMIP6.

Our analysis focuses on Tier 1 experiments (SSP1-RCP2.6, SSP2-RCP4.5, SSP3-RCP7.0 and SSP5-RCP8.5) and the additional scenario designed to limit global warming to 1.5 degree above 1850-1900 (a period often used as a proxy for pre-industrial conditions), SSP1-RCP1.9. A detailed description of these scenarios under focus is provided in Table S1.

We filtered 25 models that performed the projection of near-surface air temperature (*tas*) and near-surface relative humidity (*hurs*) to 2100. We ended up having 4 models for SSP1-RCP1.9, 16 models for SSP1-RCP2.6, 17 models for SSP2-RCP4.5, 16 models for SSP3-RCP7.0, and 17 models for SSP5-RCP8.5 to calculate Heat Index (Table S2).

2 Socioeconomic data

Total population, population by race, age and gender are county-level projections under five SSPs at a five-year interval from 2020 to 2100 (*3*). Sociodemographic data collected from multiple sources are details in Table S3. In our analysis, populations by race are categorized into non-Hispanic White, non-Hispanic Black, Hispanic (all races), and Other Races. The age groups under study are classified into Young (age below 20), Adult (age 20-64) and Elderly (age 65+). To get the downscaled data, Hauer (2019) calculates cohort-change ratios (CCRs) and cohort-change differences and projects into Leslie matrix population projection models using inputs from ARIMA models and control the projections to the SSPs.

3 Details of county-level Heat Index

The increases in Heat Index are more pronounced than the increases in surface temperature on average in the contiguous US. However, the increase in Heat Index is largely heterogeneous across the US, ranging from 0.83°F (San Benito, California) to 4.37°F (Screven, Georgia) by the middle of this century, from 2.85°F (Santa Cruz, California) to 8.53°F (Hampton, South Carolina) by the end of this century under SSP2-RCP4.5 (Fig. S3). The top 20 counties that will experience the highest increase in Heat Index are mainly located in the Southeast and their heat Indices are already as high as 80–85 °F during summer months for the baseline period. In contrast, the counties that would experience the least temperature increase are more widely distributed spatially, and most of them are located in the West region.

Fig. S1. SSP-RCP scenario matrix illustrating ScenarioMIP simulations in CMIP6 (***2***)

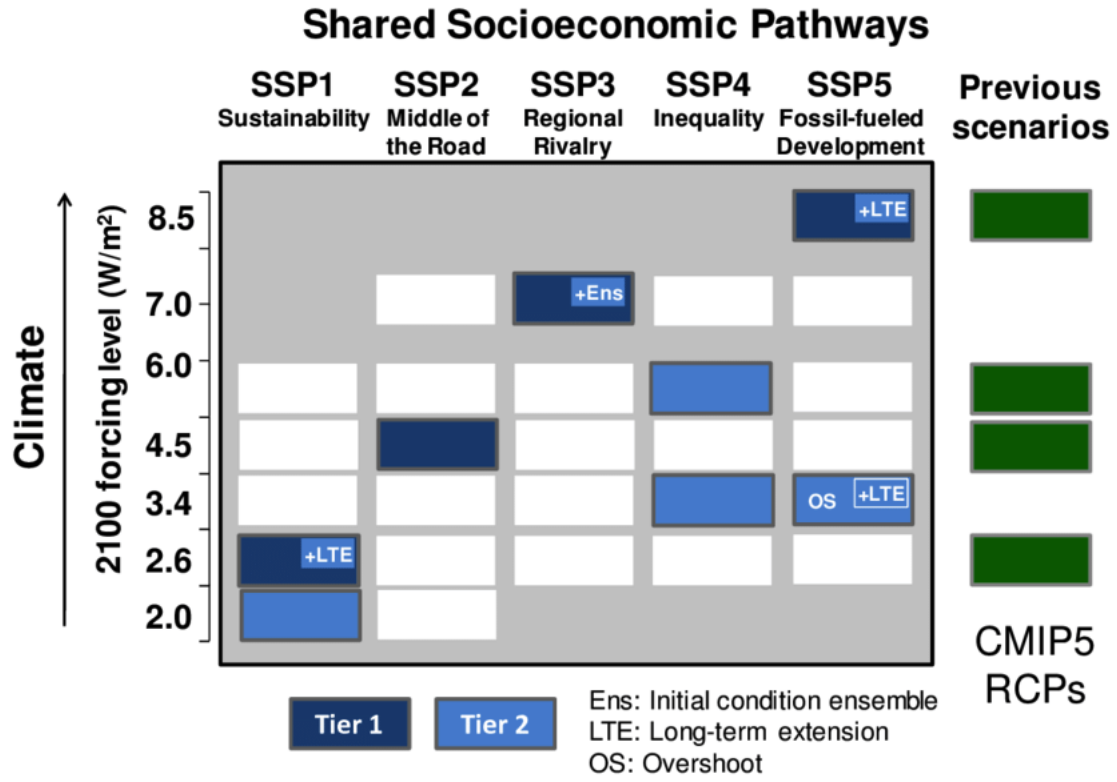

Fig. S2. Top 10 counties that would experience the highest Heat Index **(A)** in baseline period (2015-2020), **(B)** middle of the century period (2045-2050), and **(C)** end of the century period (2095-2100) under five coupled SSP-RCP scenarios

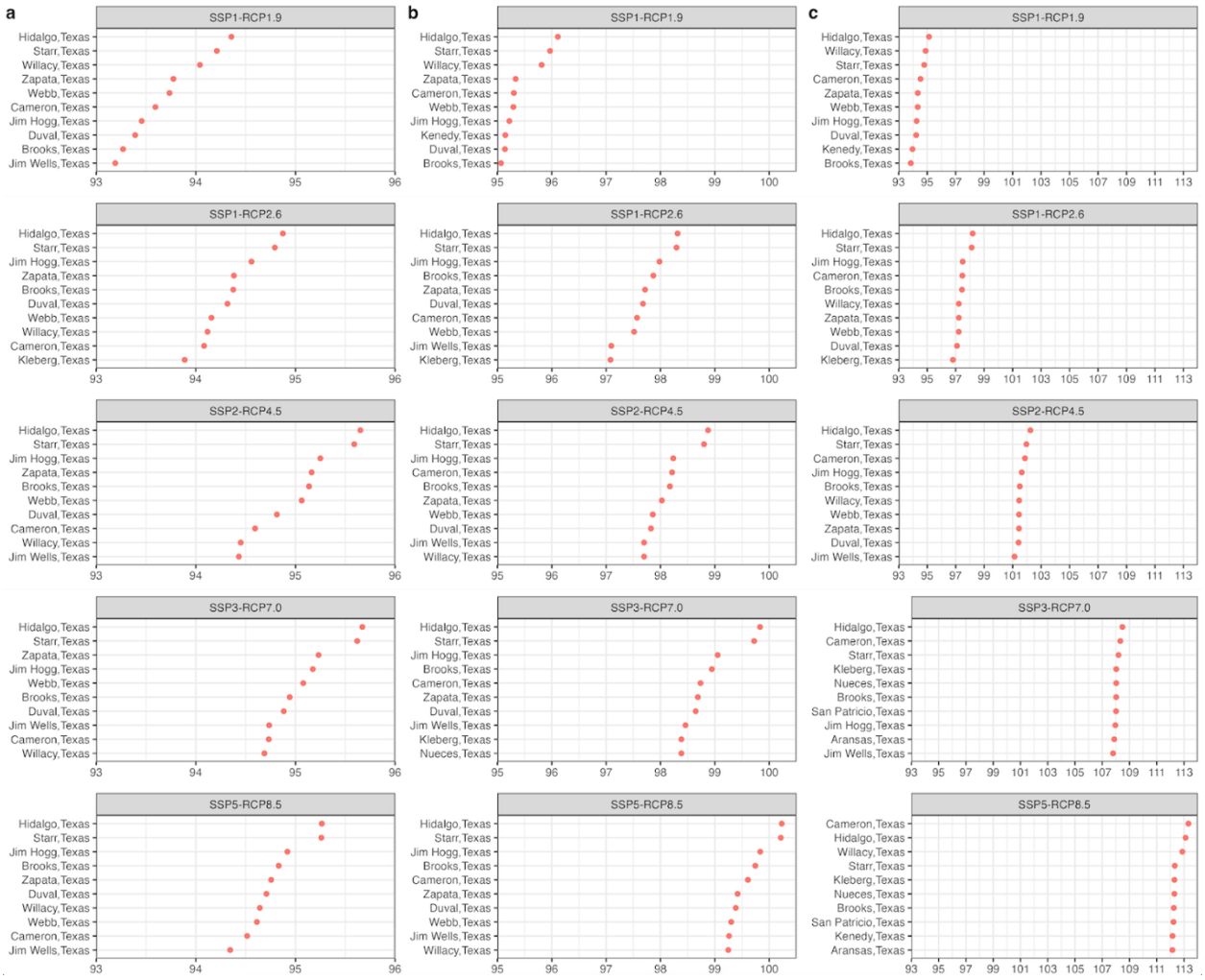

Fig. S3. Top 10 counties that would experience highest increases in Heat Index **(A)** by middle of the century period (2045-2050) and (B) by the end of the century period (2095-2100)

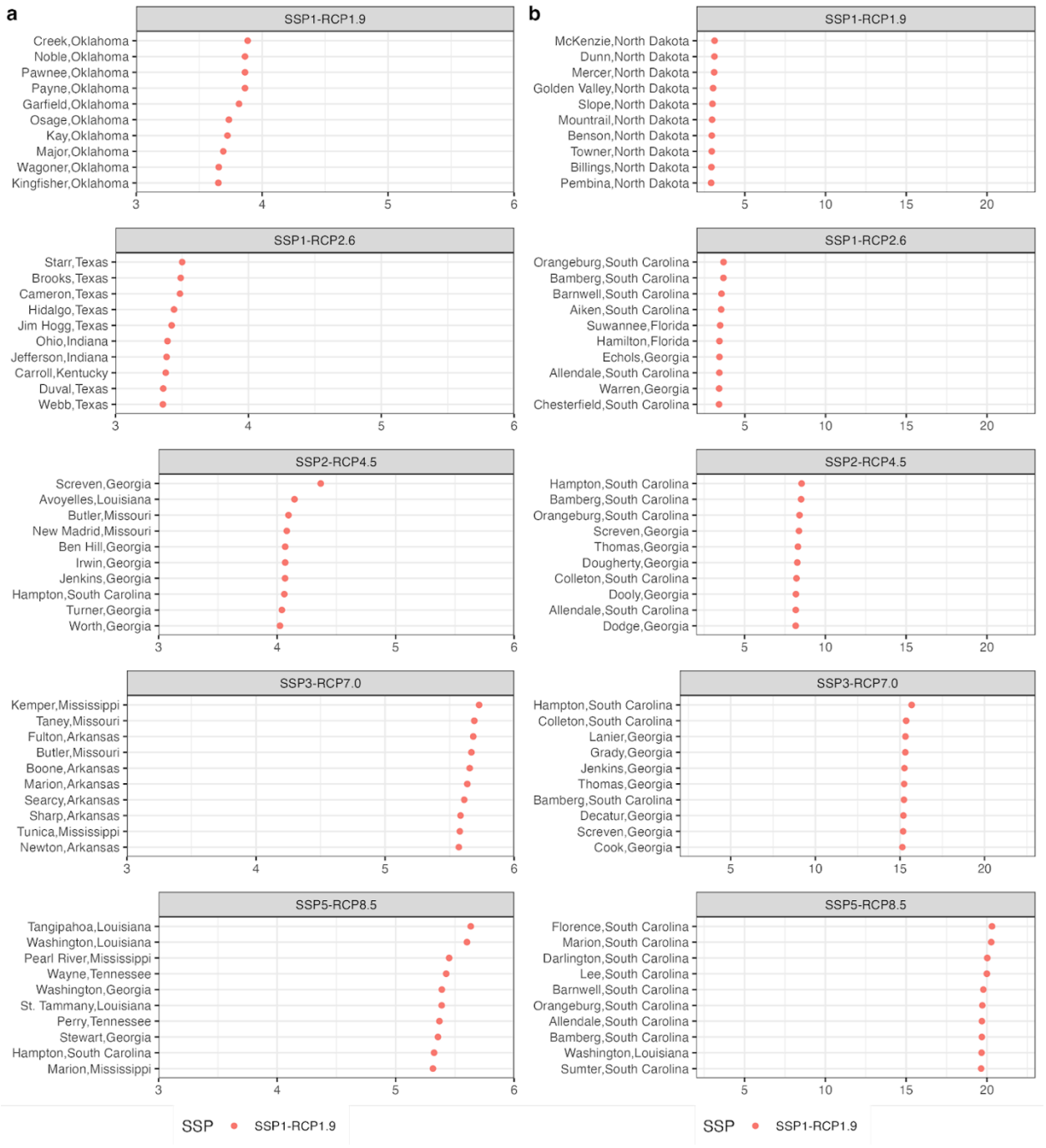

Fig. S4. Race composition for each Heat Index zone

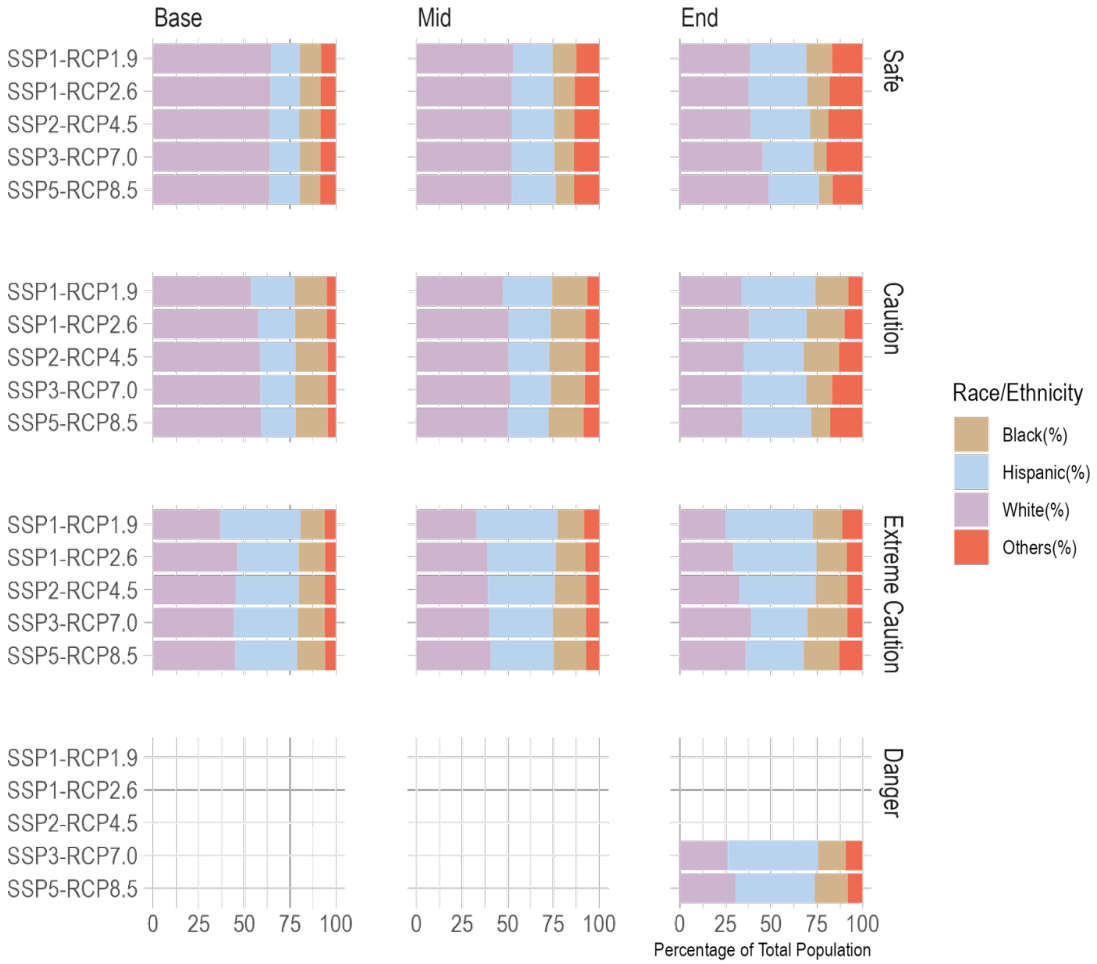

Fig. S5. Age composition for each Heat Index zone

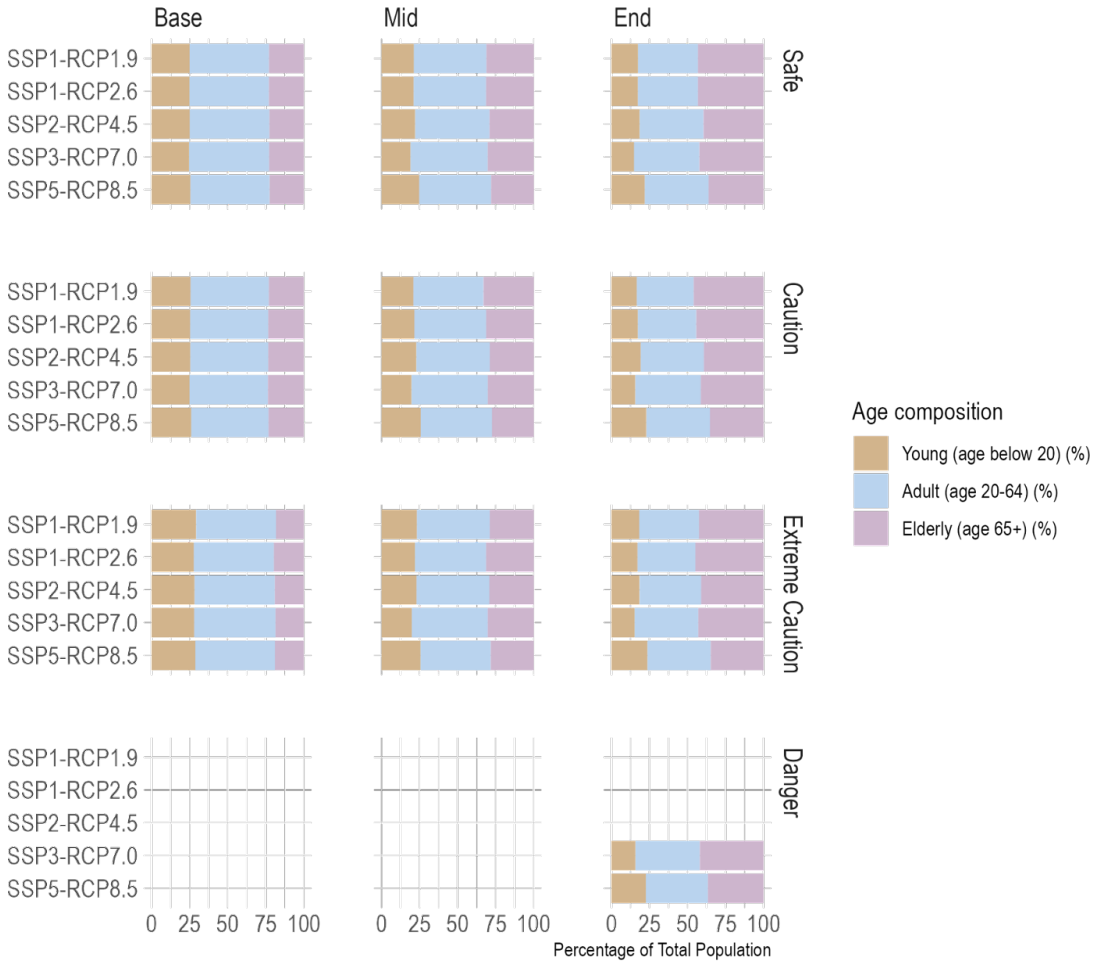

Fig. S6. Project share of non-Hispanic Black population throughout the contiguous US in five SSP scenarios for present day to 2100

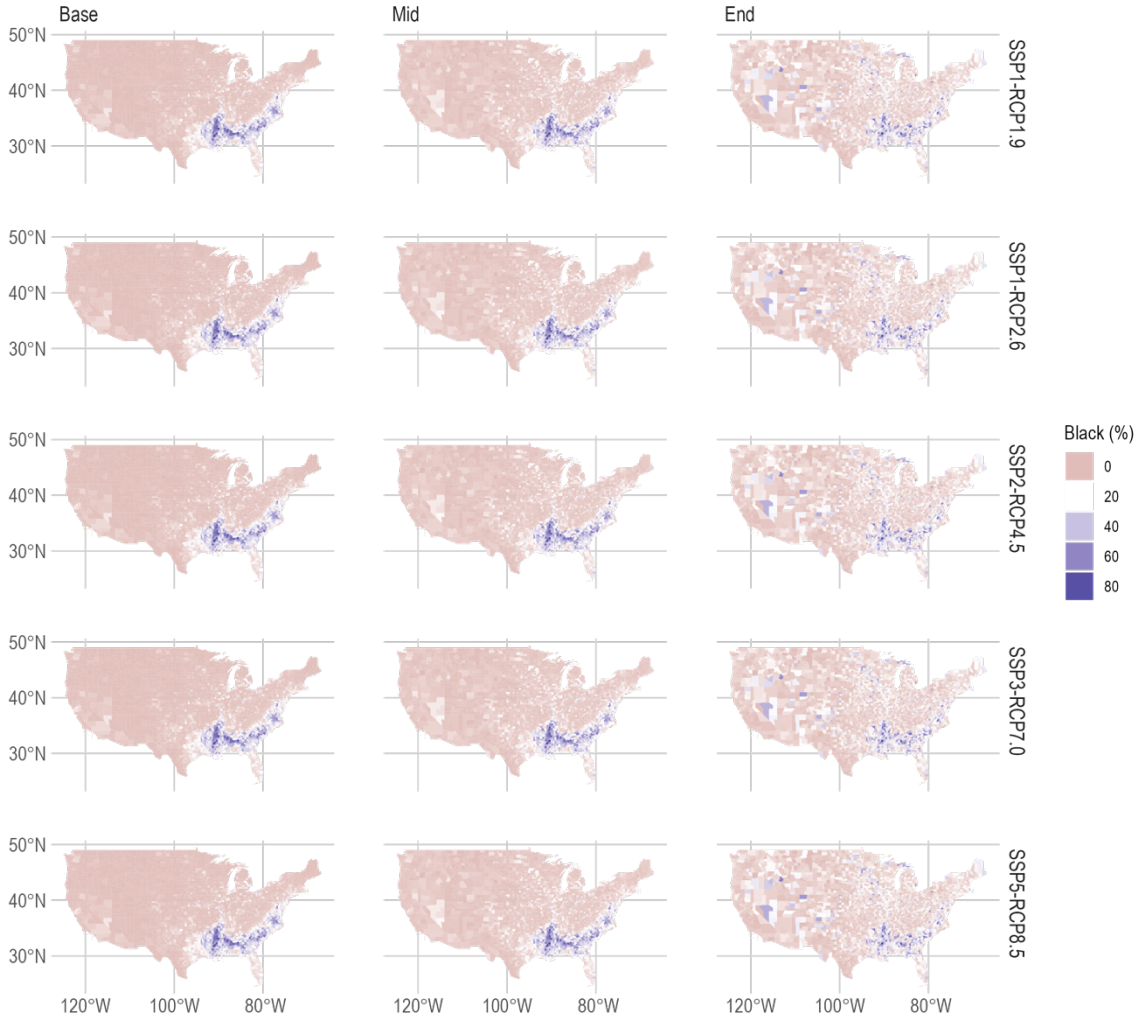

Fig. S7. Project share of Hispanic (all races) population throughout the contiguous US in five SSP scenarios for present day to 2100

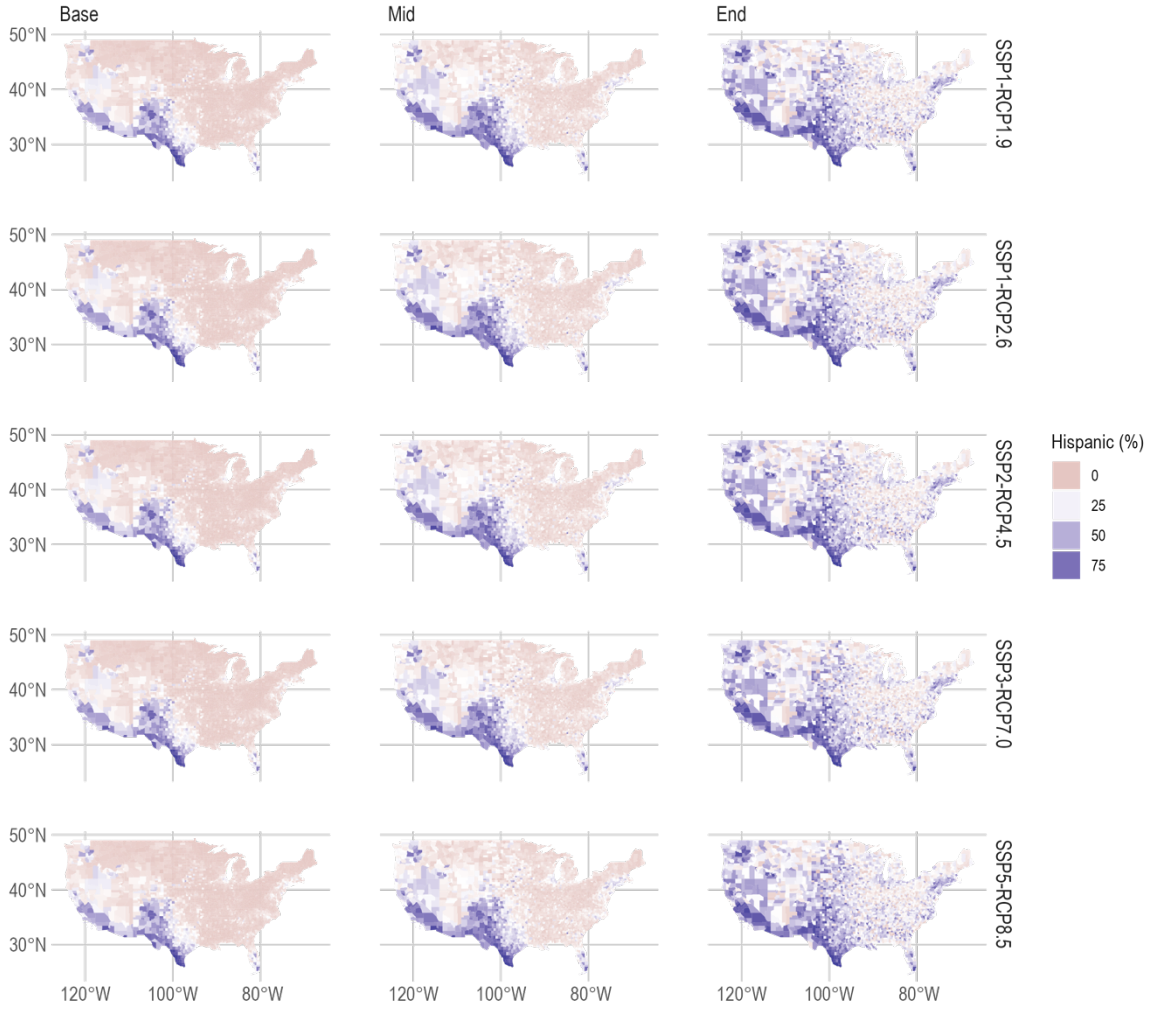

Fig. S8. Project share of Elderly (age 65+) population throughout the contiguous US in five SSP scenarios for present day to 2100

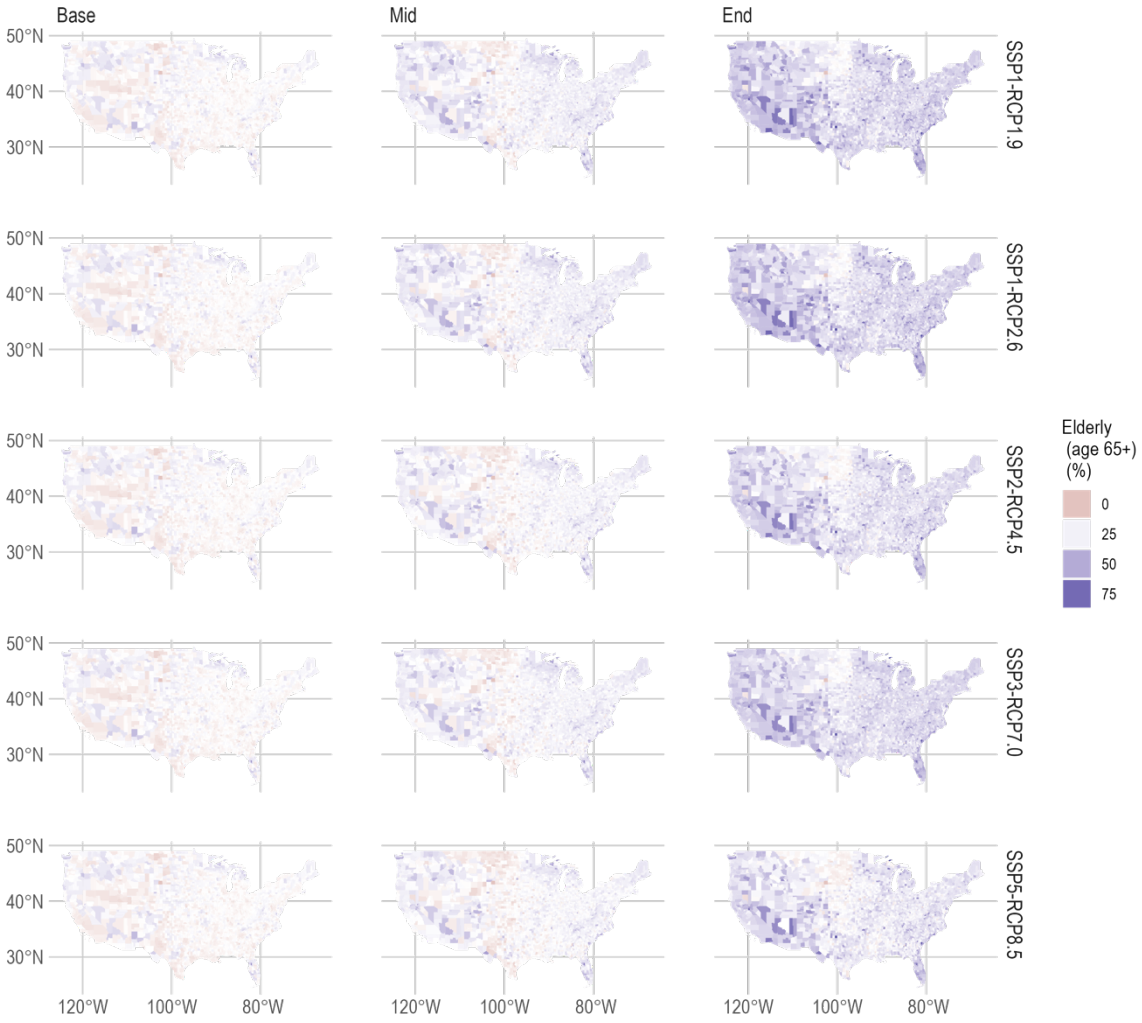

Table S1. Coupled Shared Socioeconomic Pathways (SSP) and Representative Concentration Pathways (RCP) scenarios considered in this study

SSP-RCP Pathways	Description
SSP1-RCP1.9	Very low GHG emissions: CO_2 emissions cut to net zero around 2050
SSP1-RCP2.6	Low GHG emissions: CO_2 emissions cut to net zero around 2075
SSP2-RCP4.5	Intermediate GHG emissions: CO_2 emissions around current levels until 2050, then falling but not reaching net zero by 2100
SSP3-RCP7.0	High GHG emissions: CO_2 emissions double by 2100
SSP5-RCP8.5	Very high GHG emissions: CO_2 emissions triple by 2075

Table S2. Model details from CMIP6

ID	Models	Model county	Model Institute	Resolution	Experiments	Variable		Ensemble variant
						tas	hurs	
1	AWI-CM-1-1-MR	Germany	Alfred Wegener Institute (AWI)	100km	SSP1-RCP1.9	0	0	r1i1p1
					SSP1-RCP2.6	1	1	
					SSP2-RCP4.5	1	1	
					SSP3-RCP7.0	1	1	
					SSP5-RCP8.5	1	1	
2	BCC-CSM2-MR	China	Beijing Climate Center (BCC)	100km (320 x 160 longitude/latitude)	SSP1-RCP1.9	0	0	r1i1p1
					SSP1-RCP2.6	1	0	
					SSP2-RCP4.5	1	0	
					SSP3-RCP7.0	1	0	
					SSP5-RCP8.5	1	0	
3	CAMS-CSM1-0	China	Chinese Academy of Meteorological Sciences (CAMS)	100km (320 x 160 longitude/latitude)	SSP1-RCP1.9	1	0	r1i1p1
					SSP1-RCP2.6	1	0	
					SSP2-RCP4.5	1	0	
					SSP3-RCP7.0	1	0	
					SSP5-RCP8.5	1	0	
4	CAS-ESM2-0	China	Chinese Academy of Sciences (CAS)	100km (256 x 128 longitude/latitude)	SSP1-RCP1.9	0	0	r1i1p1
					SSP1-RCP2.6	1	1	
					SSP2-RCP4.5	1	1	
					SSP3-RCP7.0	1	1	
					SSP5-RCP8.5	1	1	
5	CESM2-WACCM	USA	National Center for Atmospheric Research (NCAR)	100km (0.9x1.25 finite volume grid; 288 x 192 longitude/latitude)	SSP1-RCP1.9	0	0	r1i1p1
					SSP1-RCP2.6	1	1	
					SSP2-RCP4.5	1	1	
					SSP3-RCP7.0	1	1	
					SSP5-RCP8.5	1	1	
6	CIESM	China	Tsinghua University	100km (288 x 192 longitude/latitude)	SSP1-RCP1.9	0	0	r1i1p1
					SSP1-RCP2.6	1	0	
					SSP2-RCP4.5	1	0	
					SSP3-RCP7.0	0	0	
					SSP5-RCP8.5	1	0	
7	CMCC-CM2-SR5	Italy	Fondazione Centro Euro-Mediterraneo sui Cambiamenti Climatici (CMCC)	100km (1deg; 288 x 192 longitude/latitude)	SSP1-RCP1.9	0	0	r1i1p1
					SSP1-RCP2.6	1	1	
					SSP2-RCP4.5	1	1	
					SSP3-RCP7.0	1	1	
					SSP5-RCP8.5	1	1	
8	CMCC-ESM2	Italy	Fondazione Centro Euro-Mediterraneo sui Cambiamenti Climatici (CMCC)	100km (1deg; 288 x 192 longitude/latitude)	SSP1-RCP1.9	0	0	r1i1p1
					SSP1-RCP2.6	1	1	
					SSP2-RCP4.5	1	1	

					SSP3-RCP7.0	1	1	
					SSP5-RCP8.5	1	1	
9	E3SM-1-0	United States	E3SM-Project LLNL UCI UCSB	100km (deg average grid spacing; 90 x 90 x 6 longitude/latitude/cubeface)	SSP1-RCP1.9	0	0	r1i1p1
					SSP1-RCP2.6	0	0	
					SSP2-RCP4.5	0	0	
					SSP3-RCP7.0	0	0	
					SSP5-RCP8.5	1	0	
10	E3SM-1-1	USA	E3SM-Project; RUBISCO	100km (1 deg average grid spacing; 90 x 90 x 6 longitude/latitude/cubeface)	SSP1-RCP1.9	0	0	r1i1p1
					SSP1-RCP2.6	0	0	
					SSP2-RCP4.5	1	0	
					SSP3-RCP7.0	0	0	
					SSP5-RCP8.5	1	0	
11	E3SM-1-1-ECA	United States	E3SM-Project	100km (90 x 90 x 6 longitude/latitude/cubeface)	SSP1-RCP1.9	0	0	r1i1p1
					SSP1-RCP2.6	0	0	
					SSP2-RCP4.5	0	0	
					SSP3-RCP7.0	0	0	
					SSP5-RCP8.5	1	0	
12	EC-Earth3	Spain, Italy, Germany, UK, Finland, Switzerland	EC-Earth-Consortium	100km (linearly reduced Gaussian grid equivalent to 512 x 256 longitude/latitude)	SSP1-RCP1.9	0	0	r1i1p1
					SSP1-RCP2.6	1	1	
					SSP2-RCP4.5	1	1	
					SSP3-RCP7.0	1	1	
					SSP5-RCP8.5	1	1	
13	EC-Earth3-CC	Spain, Italy, Germany, UK, Finland, Switzerland	EC-Earth-Consortium	100km (linearly reduced Gaussian grid equivalent to 512 x 256 longitude/latitude)	SSP1-RCP1.9	0	0	r1i1p1
					SSP1-RCP2.6	0	0	
					SSP2-RCP4.5	1	1	
					SSP3-RCP7.0	0	0	
					SSP5-RCP8.5	1	1	
14	EC-Earth3-AerChem	Spain, Italy, Germany, UK, Finland, Switzerland	EC-Earth-Consortium	100km (linearly reduced Gaussian grid equivalent to 512 x 256 longitude/latitude)	SSP1-RCP1.9	0	0	r1i1p1
					SSP1-RCP2.6	0	0	
					SSP2-RCP4.5	0	0	
					SSP3-RCP7.0	1	1	
					SSP5-RCP8.5	0	0	
15	EC-Earth3-Veg	Spain, Italy, Germany, UK, Finland, Switzerland	EC-Earth-Consortium	100km (linearly reduced Gaussian grid equivalent to 512 x 256 longitude/latitude)	SSP1-RCP1.9	1	1	r1i1p1
					SSP1-RCP2.6	1	1	
					SSP2-RCP4.5	1	1	
					SSP3-RCP7.0	1	1	
					SSP5-RCP8.5	1	1	
16	EC-Earth3-Veg-LR	Spain, Italy, Germany, UK, Finland, Switzerland	EC-Earth-Consortium	100km (linearly reduced Gaussian grid equivalent to 512 x 256 longitude/latitude)	SSP1-RCP1.9	1	1	r1i1p1
					SSP1-RCP2.6	1	1	
					SSP2-RCP4.5	1	1	
					SSP3-RCP7.0	1	1	
					SSP5-RCP8.5	1	1	
17	FGOALS-f3-L	China	Chinese Academy of Sciences (CAS)	100km (360 x 180 longitude/latitude)	SSP1-RCP1.9	0	0	r1i1p1
					SSP1-RCP2.6	1	1	

					SSP2-RCP4.5	1	1	
					SSP3-RCP7.0	1	1	
					SSP5-RCP8.5	1	1	
18	FIO-ESM-2-0	China	First Institute of Oceanography, Qingdao National Laboratory for Marine Science and Technology (FIO-QLNM)	100 km (0.9x1.25 finite volume grid; 192 x 288 longitude/latitude)	SSP1-RCP1.9	0	0	r1i1p1
					SSP1-RCP2.6	1	1	
					SSP2-RCP4.5	1	1	
					SSP3-RCP7.0	0	0	
					SSP5-RCP8.5	1	1	
19	GFDL-ESM4	USA	National Oceanic and Atmospheric Administration, Geophysical Fluid Dynamics Laboratory (NOAA-GFDL)	100km (1 degree nominal horizontal resolution; 360 x 180 longitude/latitude)	SSP1-RCP1.9	1	1	r1i1p1
					SSP1-RCP2.6	1	1	
					SSP2-RCP4.5	1	1	
					SSP3-RCP7.0	1	1	
					SSP5-RCP8.5	1	1	
20	INM-CM4-8	Russia	Institute for Numerical Mathematics (INM)	100km (2x1.5; 180 x 120 longitude/latitude; 21 levels; top level sigma = 0.01))	SSP1-RCP1.9	0	0	r1i1p1
					SSP1-RCP2.6	1	1	
					SSP2-RCP4.5	1	1	
					SSP3-RCP7.0	1	1	
					SSP5-RCP8.5	1	1	
21	INM-CM5-0	Russia	Institute for Numerical Mathematics (INM)	100km (2x1.5; 180 x 120 longitude/latitude; 73 levels; top level sigma = 0.0002)	SSP1-RCP1.9	0	0	r1i1p1
					SSP1-RCP2.6	1	1	
					SSP2-RCP4.5	1	1	
					SSP3-RCP7.0	1	1	
					SSP5-RCP8.5	1	1	
22	MPI-ESM1-2-HR	Germany	Max Planck Institute for Meteorology (MPI-M); Deutscher Wetterdienst (DWD); Deutsches Klimarechenzentrum (DKRZ)	100km (spectral T127; 384 x 192 longitude/latitude; 95 levels; top level 0.01 hPa)	SSP1-RCP1.9	0	0	r1i1p1
					SSP1-RCP2.6	1	1	
					SSP2-RCP4.5	1	1	
					SSP3-RCP7.0	1	1	
					SSP5-RCP8.5	1	1	
23	MRI-ESM2-0	Japan	Meteorological Research Institute (MRI)	100km (320 x 160 longitude/latitude; 80 levels; top level 0.01 hPa)	SSP1-RCP1.9	1	1	r1i1p1
					SSP1-RCP2.6	1	1	
					SSP2-RCP4.5	1	1	
					SSP3-RCP7.0	1	1	
					SSP5-RCP8.5	1	1	
24	TaiESM1	Taiwan	Research Center for Environmental Changes, Academia Sinica (AS-RCEC)	100km (0.9x1.25 degree; 288 x 192 longitude/latitude; 30 levels; top level ~2 hPa)	SSP1-RCP1.9	0	0	r1i1p1
					SSP1-RCP2.6	1	0	
					SSP2-RCP4.5	1	0	
					SSP3-RCP7.0	1	0	
					SSP5-RCP8.5	1	0	
25	NorESM2-MM	Norway	Norwegian Climate Centre (NCC)	100km (1 degree resolution; 288 x 192; 32 levels; top level 3 mb)	SSP1-RCP1.9	0	0	r1i1p1
					SSP1-RCP2.6	1	1	
					SSP2-RCP4.5	1	1	
					SSP3-RCP7.0	1	1	

					SSP5-RCP8.5	1	1	

Note: "tas" denotes near-surface air temperature (2m above the ground), "hurs" denotes relative humidity, data sources: https://github.com/WCRP-CMIP/CMIP6_CVs/blob/master/README.md

Table S3. Downscaled Sociodemographic data and their sources

Socioeconomic factors	Data source	Original spatial resolution	Reference
Urban fraction	Gao et al. (2021)	1/8 degree	*(4)*
Population	Socioeconomic Data and Applications Center (SEDAC)	US county	*(3)*
Gender	Socioeconomic Data and Applications Center (SEDAC)	US county	*(3)*
Race	Socioeconomic Data and Applications Center (SEDAC)	US county	*(3)*
Age	Socioeconomic Data and Applications Center (SEDAC)	US county	*(3)*
Income	Murakami	1/12 degree	(*5*)

Table S4. Probability of having heat disorders with prolonged exposure (summer average HI>80F)

Month	2020	2050	2100	Increase in likelihood of heat disorders (2020-2050)	Increase in likelihood of heat disorders (2020-2100)
Jan	0.00	0.00	0.04	0.00	0.04
Feb	0.00	0.00	0.04	0.00	0.04
Mar	0.00	0.01	0.12	0.01	0.12
Apr	0.04	0.10	0.22	0.05	0.18
May	0.19	0.27	0.44	0.08	0.26
Jun	0.35	0.45	0.63	0.10	0.28
Jul	0.47	0.56	0.75	0.09	0.28
Aug	0.47	0.57	0.75	0.10	0.28
Sep	0.32	0.41	0.63	0.09	0.31
Oct	0.17	0.24	0.42	0.07	0.25
Nov	0.04	0.10	0.24	0.06	0.20
Dec	0.00	0.00	0.12	0.00	0.12

Table S5. Population movement between Heat Index zones in 2050 and 2100

Coupled SSP-RCP scenarios	2050			2100					
	No movement (%)	Safe to Caution (%)	Caution to Extreme Caution (%)	No movement (%)	Safe to Caution (%)	Caution to Extreme Caution (%)	Extreme Caution to Danger (%)	Caution to Danger (%)	Safe to Extreme Caution (%)
SSP1-1.9	91.4 (90.7)	2.3 (4.9)	6.2 (4.4)	94.9 (94.0)	2.1 (4.6)	2.9 (1.4)	NA	NA	NA
SSP1-2.6	87.4 (84.8)	6.1 (9.7)	6.5 (5.5)	86.0 (84.4)	6.8 (10.3)	7.2 (5.3)	NA	NA	NA
SSP2-4.5	81.2 (78.9)	10.3 (13.4)	8.5 (7.7)	59.0 (55.3)	26.2 (25.6)	14.9 (19.0)	NA	NA	NA
SSP3-7.0	78.8 (73.6)	11 (15.6)	10.2 (10.7)	17.4 (17.0)	45.7 (37.6)	22 (32.2)	8.9 (5.8)	1.8 (0.8)	4.3 (6.6)
SSP5-8.5	72.7 (72.0)	14.9 (15.4)	12.4 (12.5)	7.2 (8.0)	35.5 (27.8)	15.1 (24.4)	9.6 (7.1)	11.2 (12.6)	21.4 (20.0)

Note: the numbers show the percentage of population and number of counties using 2020 as reference, the percentage does not add up to 100%

Table S6. Population-weighted Heat Index by race under four coupled SSP-RCP scenarios

Race	SSP-RCP	2020	2050	2100
White NH	SSP1-RCP2.6	77.0	79.6	80.3
Black NH	SSP1-RCP2.6	80.0	82.5	82.7
Hispanic	SSP1-RCP2.6	80.2	82.6	82.7
Others	SSP1-RCP2.6	76.5	78.7	79.0
White NH	SSP2-RCP4.5	77.1	80.1	83.7
Black NH	SSP2-RCP4.5	79.9	83.1	86.4
Hispanic	SSP2-RCP4.5	80.2	83.0	86.0
Others	SSP2-RCP4.5	76.5	79.1	82.0
White NH	SSP5-RCP8.5	77.4	81.4	93.3
Black NH	SSP5-RCP8.5	80.4	84.5	96.8
Hispanic	SSP5-RCP8.5	80.4	84.1	95.3
Others	SSP5-RCP8.5	76.7	80.2	91.0
White NH	SSP3-RCP7.0	76.8	80.6	88.7
Black NH	SSP3-RCP7.0	79.8	83.7	91.8
Hispanic	SSP3-RCP7.0	80.1	83.5	91.0
Others	SSP3-RCP7.0	76.3	79.4	86.6

Note: NH denotes non-Hispanic

Table S7. US Census Regions in the contiguous United States

State	State Code	Region
Alabama	AL	South
Arkansas	AR	South
Arizona	AZ	West
California	CA	West
Colorado	CO	West
Connecticut	CT	Northeast
District of Columbia	DC	South
Delaware	DE	South
Florida	FL	South
Georgia	GA	South
Iowa	IA	Midwest
Idaho	ID	West
Illinois	IL	Midwest
Indiana	IN	Midwest
Kansas	KS	Midwest
Kentucky	KY	South
Louisiana	LA	South
Massachusetts	MA	Northeast
Maryland	MD	South
Maine	ME	Northeast
Michigan	MI	Midwest
Minnesota	MN	Midwest
Missouri	MO	Midwest
Mississippi	MS	South
Montana	MT	West
North Carolina	NC	South
North Dakota	ND	Midwest
Nebraska	NE	Midwest
New Hampshire	NH	Northeast
New Jersey	NJ	Northeast
New Mexico	NM	West
Nevada	NV	West
New York	NY	Northeast
Ohio	OH	Midwest
Oklahoma	OK	South
Oregon	OR	West
Pennsylvania	PA	Northeast
Rhode Island	RI	Northeast
South Carolina	SC	South
South Dakota	SD	Midwest
Tennessee	TN	South
Texas	TX	South
Utah	UT	West
Virginia	VA	South
Vermont	VT	Northeast
Washington	WA	West
Wisconsin	WI	Midwest

West Virginia	WV	South
Wyoming	WY	West

References

1. C. Tebaldi, K. Debeire, V. Eyring, E. Fischer, J. Fyfe, P. Friedlingstein, R. Knutti, J. Lowe, B. O'Neill, B. Sanderson, D. van Vuuren, K. Riahi, M. Meinshausen, Z. Nicholls, K. B. Tokarska, G. Hurtt, E. Kriegler, J.-F. Lamarque, G. Meehl, R. Moss, S. E. Bauer, O. Boucher, V. Brovkin, Y.-H. Byun, M. Dix, S. Gualdi, H. Guo, J. G. John, S. Kharin, Y. Kim, T. Koshiro, L. Ma, D. Olivié, S. Panickal, F. Qiao, X. Rong, N. Rosenbloom, M. Schupfner, R. Séférian, A. Sellar, T. Semmler, X. Shi, Z. Song, C. Steger, R. Stouffer, N. Swart, K. Tachiiri, Q. Tang, H. Tatebe, A. Voldoire, E. Volodin, K. Wyser, X. Xin, S. Yang, Y. Yu, T. Ziehn, Climate model projections from the Scenario Model Intercomparison Project (ScenarioMIP) of CMIP6. *Earth System Dynamics*. **12**, 253–293 (2021).
2. B. C. O'Neill, C. Tebaldi, D. P. van Vuuren, V. Eyring, P. Friedlingstein, G. Hurtt, R. Knutti, E. Kriegler, J.-F. Lamarque, J. Lowe, G. A. Meehl, R. Moss, K. Riahi, B. M. Sanderson, The Scenario Model Intercomparison Project (ScenarioMIP) for CMIP6. *Geosci Model Dev*. **9**, 3461–3482 (2016).
3. M. E. Hauer, Population projections for U.S. counties by age, sex, and race controlled to shared socioeconomic pathway. *Sci Data*. **6**, 190005 (2019).
4. J. Gao, M. Pesaresi, Downscaling SSP-consistent global spatial urban land projections from 1/8-degree to 1-km resolution 2000–2100. *Sci Data*. **8**, 281 (2021).
5. D. Murakami, T. Yoshida, Y. Yamagata, Gridded GDP Projections Compatible With the Five SSPs (Shared Socioeconomic Pathways). *Front Built Environ*. **7** (2021), doi:10.3389/fbuil.2021.760306.